Chapter 12

Changes in Visual Cortex in Healthy Aging and Dementia

Alyssa A. Brewer and Brian Barton

Additional information is available at the end of the chapter

http://dx.doi.org/10.5772/64562

Abstract

This chapter reviews the differences in specific structural and functional characteristics of human visual cortex among young adults, healthy aging adults, and patients with dementia, with a primary focus on those with Alzheimer's disease (AD). Such visual cortex changes have been shown to underlie many of the behavioral deficits that develop in healthy aging and AD. Measurements of disordered visual cortex in dementia patients may be possible early in the course of neurodegeneration and thus may be useful for improving early diagnosis of these devastating diseases.

Keywords: visual cortex, visual field mapping, dementia, healthy aging, functional neuroimaging

1. Introduction

1.1. Overview of visual cortex characteristics

Human visual cortex can be partitioned into distinct topographical representations of visual space called visual field maps (VFMs), each of which subserves separate perceptual functions spanning the hierarchical stages of visual processing [1–3]. The organization of a VFM follows the organization of the retina; hence, retinotopic VFMs are cortical regions in which nearby neurons analyze the properties of nearby points of an image on the retina, and thus of visual space. This VFM organization is one of the more important, larger-scale, organizing principles of visual cortex. Such topographic organization is thought to allow for efficient connectivity among neurons that represent nearby aspects of visual space, likely necessary for such processes as lateral inhibition and to compactly organize neural signals ranging from the molecular level to that of the cerebral hemisphere [4–7]. In addition, measurements of the characteristics of these VFMs, together with an understanding of the stimulus selectivity of the

neurons within them, is the foundation for understanding the specific visual computations carried out in particular cortical regions. Not only are such *in vivo* measurements of VFMs essential for the study of visual processing in healthy subjects, but they also are very effective for tracking changes in visual cortex in response to changes in visual inputs such as those that arise from retinal or cortical damage [8–12].

Although historically the organization and function of visual cortex have been primarily well characterized in healthy young adults or young patient populations [1–3, 8, 12–16], many behavioral studies [17–38] and more recent neuroimaging studies [36, 37, 39–55] are suggesting that several changes occur within visual pathways during what is considered otherwise healthy aging. These studies specifically describe retinal and cortical changes, rather than optical changes in the eye, that primarily contribute to the decreases in visual acuity and related issues that have been measured in healthy aging subjects [19, 33, 46, 50, 54]. These healthy aging changes are also now starting to be compared to pathophysiological changes in visual cortex in age-related disorders like dementia, including diseases such as Alzheimer's disease (AD), posterior cortical atrophy (PCA), and dementia with Lewy bodies (DLB), in the hopes of both improving our understanding of these diseases and aiding improvements in potential therapies [37, 56].

Visual deficits are reported surprisingly often as one of the first symptoms of AD, the most common form of dementia. These deficits can include problems with visual-spatial attention, visual-spatial tasks, and visual-processing speed [37, 40, 47, 57–75]. A subset of dementia patients presents with prominent visual symptoms such as problems with visual field defects, contrast sensitivity, color discrimination, and feature recognition of complex objects, but little initial decline in memory. These patients have increased neuropathology in visual cortex, as compared to typical AD patients [76–84]. Dementia with these characteristics was initially often referred to as visual variant AD, but it is now usually termed PCA. DLB, the second most common type of dementia, also often presents with visual complaints [85]. Like in AD and PCA, the central features of DLB include progressive cognitive decline, typically with impairments in memory, visual-spatial abilities, and attention. However, unlike AD and PCA, one of the earliest visual symptoms in this disease is commonly visual hallucination [86].

Early detection and accurate diagnosis are keys in the hope for a cure for such dementias, as early, precise diagnosis would allow for more timely initiation of treatments. As visual symptoms can occur early in these diseases, studies are beginning to demonstrate that measurements of related changes in visual cortex in these patients could aid early detection of neurodegeneration. The highly structured representations within VFMs afford a fundamental measurement that might be used to detect subtle effects of neurodegeneration early in the disease process. Clear measures of the progression of the pathology within visual cortex might also help to target drug research for therapeutic interventions, especially by differentiating among different types of dementia [62]. The information reviewed in this chapter will serve as a foundation for subsequent use of this knowledge in our evaluation, interpretation, and treatment of these diseases. As little has been studied regarding VFMs in patients with PCA or DLB, this chapter will focus on measurements from patients with AD.

http://dx.doi.org/10.5772/64562

1.2. Review methodology

We performed a systematic review to investigate whether there are changes in early VFMs V1, V2, V3, and hV4 characteristics to healthy aging subjects and patients with AD or related dementias that can be measured using functional magnetic resonance imaging (fMRI). In order to include as many relevant citations as possible, we searched a comprehensive range of scientific databases including CogPrints, FreeFullPDF, Google Scholar, IngentaConnect, JSTOR, Mendeley, Microsoft Academic Search, PubMed, PubPsych, ResearchGate, and Web of Science. In addition, the Google search engine was used to find institutional, professional, and personal webpages hosting potentially relevant PDFs or citation links. Searches were performed from November 2015, to May 2016. Search queries included the following terms in various combinations: visual cortex, visual field map, visual area, primary visual cortex, V1, V2, V3, hV4, occipital cortex, visual changes, fMRI, pRF modeling/modeling, neuroimaging, aging, healthy aging, human, dementia, neurodegeneration, mild cognitive impairment, Alzheimer's disease, dementia with Lewy bodies, Lewy body dementia, and posterior cortical atrophy. Related citation links available for the various database searches were routinely evaluated to investigate additional potential citations of interest. All potential study designs were included, and potentially relevant citations spanned the dates 1925–2016; note that visual field mapping with fMRI was relatively recently introduction in 1994 [87].

Ultimately, 317 potentially relevant citations were downloaded to EndNote for further evaluation. The full papers of these citations were assessed and selected to only include studies that directly related to comparing fMRI measures of visual cortex or visual field maps in healthy young adults (aged 18–40 years) to changes in visual cortex or visual field maps in healthy aging subjects with no known age-related diseases or specific, clinically recognized deficits in vision (aged 55–80 years) and/or to patients with mild-to-moderate AD with no known visual deficits unrelated to dementia (aged 55–80 years). No studies of VFM changes in DLB or PCA were found during the initial database searches, which was not unexpected given the very recent emergence of interest in visual field mapping in dementia. Additional studies of visual field mapping methodology and of visual symptoms associated with healthy aging, AD, DLB, and PCA were also retained for methods discussion and hypothesis development, respectively. Studies were further evaluated for quality and were excluded if they lacked statistical analysis or if they did not use accurate cortical field mapping techniques with individual subject analysis (for further discussion of these criteria, see [1, 3, 88]).

Of the 317 downloaded studies, 165 papers were directly relevant to this review, of which 88 focused on visual changes in aging or dementia. Of these, 24 studies measured changes specifically in visual cortex related to aging and/or dementia, and three studies explicitly investigated VFM changes in aging and/or dementia, as appropriate with respect to the inclusion and exclusion criteria [36, 37, 39]. Here, we provide both a narrative discussion of all 165 sources as well as graphical examples drawn from the three key visual field mapping studies. We discuss what is known regarding changes in early visual cortex during healthy aging and AD, how these findings relate to visual symptoms in these conditions, and what remains to be studied, and we recommend directions for future research.

2. The measurement and organization of visual cortex in healthy young adults

In order to carefully evaluate alterations of visual cortex in healthy aging and age-related neurodegenerative diseases such as AD, we must first have an accurate and detailed understanding of the characteristics of visual cortex in healthy young adults. Visual cortex encompasses nearly 20% of the human cortical sheet, and studies are demonstrating that nearly all of it is organized into VFMs [1, 3]. Because many calculations are necessary to produce our visual world, our brains have many specialized VFMs which perform one or more of those calculations [3, 89]. Most—if not all—of these calculations are performed across the entire visual scene; color perception, for example, occurs throughout the visual field, not just in the lower right quadrant. Ultimately, it will be very interesting to investigate changes in visual cortex among all levels of the cortical visual hierarchy, from low-level visual processing in primary visual cortex (V1) to mid-level specialization like motion processing to higher-level processing like face recognition and visual-spatial attention [2, 90]. For now, studies of plasticity and neurodegeneration primarily investigate the lower level visual areas like V1, V2, V3, and hV4, as these VFMs are particularly well established in healthy young adults, relatively uncontroversial, and typically easily measured across most types of patients [1, 3, 8, 12, 14, 15, 37, 91].

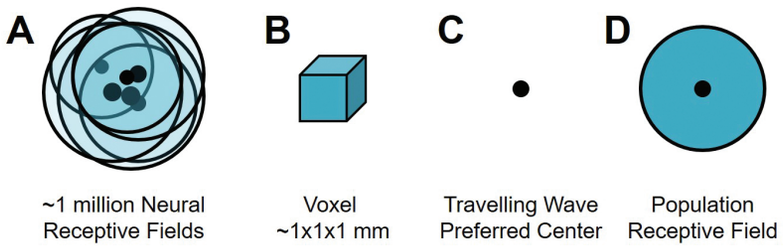

Figure 1. Schematic of measurements of an individual voxel. (A) Within a typical voxel measured with a standardly used 3T MRI scanner, there are on the order of ~1 million neurons, depending on the size of the voxel. For voxels in retinotopic visual cortex, the neurons each have similarly located spatial receptive fields (*teal circles with black outlines*) with preferred centers (*black dots*). Note how the overlapping receptive fields concentrate coverage in one region of visual space (*darker teal*) corresponding to the average receptive field of the group, as shown in **(D)**. **(B)** Each typical voxel is on the order of 1 × 1 × 1 mm for structural measurements and 1 × 1 × 3 mm for visual field mapping functional experiments, though voxels are often slightly larger (e.g., 3 × 3 × 3 mm) for other types of functional MR studies. **(C)** Traveling wave retinotopy (TWR) utilizes the organization of retinotopic cortex, in which neighboring neurons have preferred centers (*black dot*) representing similar portions of visual space, to estimate the average preferred representation (center) for the population of neurons in a given voxel (e.g., [1, 3]). **(D)** Population receptive field (pRF) modeling similarly utilizes retinotopic organization to estimate not only the preferred center (*black dot*) in a given voxel, but also the average receptive field—the population receptive field (*teal circle*)—for the voxel's population of neurons (e.g., [1, 3, 92]).

2.1. Human visual field map measurements use simple stimuli and tasks, but provide exquisite detail of cortical organization

We briefly review here two of the most powerful fMRI techniques for very detailed measurements of VFMs in individual subjects, traveling wave retinotopy (TWR) [87] and population

receptive field (pRF) modeling [92], to demonstrate what types of measurements are possible and how to interpret the existing literature regarding changes in aging or damaged visual cortex (**Figures 1–4**).

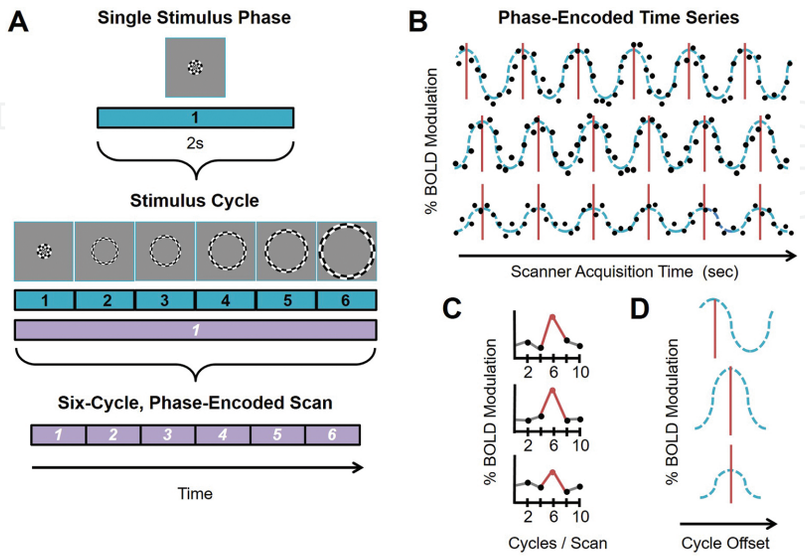

Figure 2. Phase-encoded fMRI paradigm for visual field map measurements. (A) An example phase-encoded experimental design [87]. Top diagram shows the components of a single block of one stimulus presentation (*teal*) for one position (i.e., stimulus phase) of an expanding ring stimulus composed of a black and white moving checkerboard pattern. Middle diagram shows six blocks (*teal*) grouped together into one stimulus cycle (*purple*). The progressively larger ring stimulus is shown above each block. Each block in one cycle presents a specific stimulus in the "phase-encoded"—or "traveling wave"—sequence. Each cycle then repeats the same set of blocks. Lower diagram shows a full, single scan comprising six cycles; each cycle is one purple block. **(B)** Schematic diagram of three example phase-encoded time series with different stimulus responses. Each row depicts the time series measurement for a single voxel arising from a single, six-cycle scan using one experimental stimulus (e.g., polar angle). Simulated raw data points showing percent blood-oxygen-level-dependent (BOLD) modulation (i.e., response amplitude) are denoted by the black dots. The teal dotted lines represent sinusoidal fits of the simulated data points; each teal line characterizes the average BOLD activation in a different example voxel. The red lines indicate the peak activations per cycle for this imaginary set of voxels. Top and middle rows represent time series of voxels with the same %BOLD modulation, but different timing of peak responses, which indicates different stimulus selectivity (i.e., responses to different "phases" of the stimulus). Note the offset of the red lines between the two rows. For example, the top row might represent a voxel with a preferred eccentricity tuning of 2° eccentric to fixation, whereas the middle row might have a preferred tuning of 5° eccentric to fixation. Middle and bottom rows represent time series of voxels with the same timing of peak responses, indicating matching stimulus selectivity; i.e., both might have a preferred eccentricity tuning of 5° eccentric to fixation. However, the bottom row has much lower %BOLD modulation than the middle row. Such a difference in response amplitude can be due to several factors, such as differences in local vasculature or receptive field tuning. **(C)** Diagram of three example Fourier power spectra corresponding to the schematic time series in **(B)**. In the phase-encoded paradigm, only BOLD responses that match the stimulus frequency of six cycles per scan (*red peak*) are considered as data. The responses must also be above a predetermined statistical threshold, typically measured in coherence or percentage variance explained [3, 87, 92]. **(D)** Diagram of three example averaged stimulus cycles corresponding to the schematic Fourier spectra in **(C)** and to averages of the time series in **(B)**. Each teal dotted line represents the sinusoidal fit for the average, while the peak activation is again marked by the red line. The timing of the peak of each averaged cycle is used to calculate the phase of the preferred stimulus independently for each voxel. Typical pseudocolor overlays on 3D or flattened brain renderings as shown in **Figures 6** and **12** use color to denote cortical responses to this peak activation. Note how the top measurement has an earlier peak (*red line*) that corresponds to an earlier phase of the stimulus (i.e., an earlier presentation time in the cycle) while the middle and bottom measurements' peaks are shifted to later in time (e.g., [3]). The bottom example has a lower %BOLD modulation than the other two schematics, but the same peak activation as the middle example. For additional discussion, see [1, 3, 87, 91, 92].

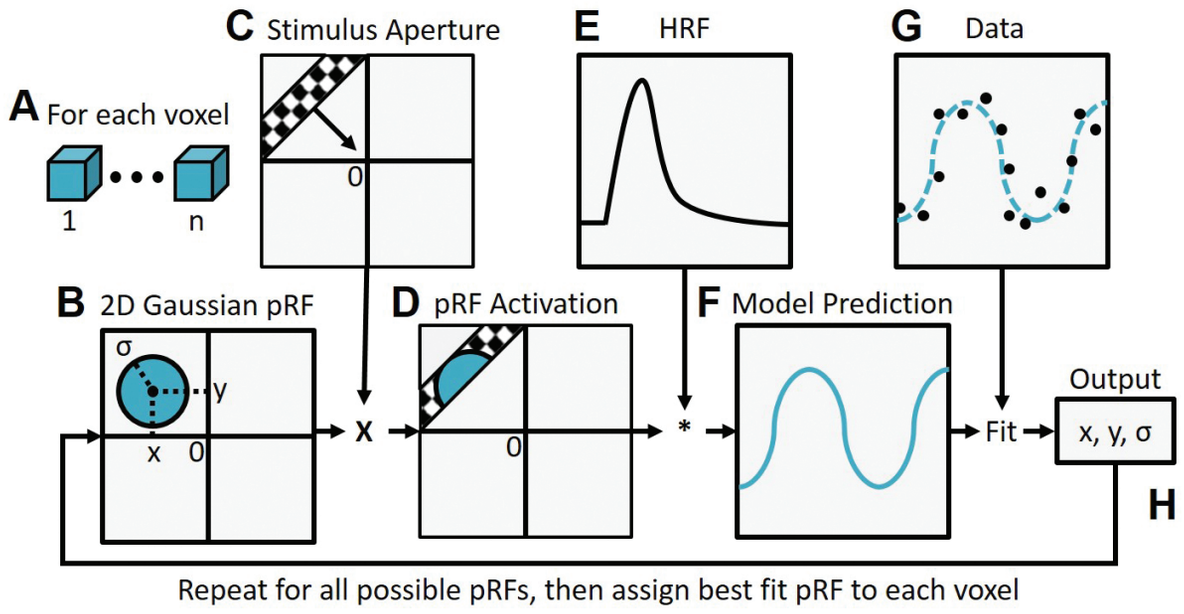

Figure 3. Population receptive field modeling. The parameter estimation procedure for the population receptive field (pRF) model is shown as a flow chart [92]. The pRF parameters are estimated from time series measurements using a linear spatiotemporal model of the fMRI response, which is a reasonable approximation over a wide range of spatiotemporal conditions [94–96]. The neuronal model is estimated by finding the model parameters that best predict the fMRI measurements. **(A)** The pRF modeling analysis is applied to all voxels (1:*n*) within the defined region of interest (ROI; e.g., occipital lobe, V1). **(B)** Multiple models of the expected average receptive field of the neuronal population may be used. Most commonly, a two-dimensional Gaussian is estimated, which is defined by three parameters, *x*, *y*, and *σ*, where (*x*, *y*) denotes the pRF center within the visual field, and *σ* is the Gaussian spread (i.e., pRF radius). Note that these parameters are stimulus-referred in degrees of visual angle. **(C)** The example moving bar stimulus composed of a black and white moving checkerboard pattern moves systematically across visual space. **(D)** The overlap between the pRF and effective stimulus is determined. **(E, F)** Next, the predicted pRF response is calculated for a given pRF model and effective stimulus location. The time series model prediction **(F)** is estimated by convolving the pRF activation with a model of the hemodynamic response function (HRF) as in **(E)** [94, 97]. The goodness-of-fit is estimated by computing the residual sum of squares (RSS) between this prediction and the data (*black dots*) **(G)**. **(H)** 100,000 different fMRI time series predictions are iteratively tested by varying the pRF model parameters across a wide range of plausible values (e.g., locations across visual space covered by the stimulus; varying pRF sizes). Ultimately, the optimal pRF parameters (*x*, *y*, *σ*) are found for each voxel independently by minimizing the RSS using a two-stage, coarse-to-fine search. Adapted from **Figure 2** in [92].

2.1.1. Traveling wave retinotopy

Developed in the 1990s, TWR is still the primary fMRI paradigm used to measure early VFMs like V1–3 (**Figures 1** and **2**) [13, 15, 87, 91, 93]. This technique uses two types of periodic stimuli that move smoothly across a contiguous region of visual space to measure the orthogonal dimensions of polar angle (i.e., "around the clock") and eccentricity (i.e., center to periphery; **Figure 5**). These stimuli are typically composed of a set of high-contrast, flickering checkerboard patterns that are designed to maximally stimulate primary visual cortex and generally elicit an fMRI signal modulation on the order of 1–3% (**Figure 2A**). This modulation is typically 15–20 standard deviations above the background noise. Each voxel's preferred polar angle representation is measured by a rotating wedge stimulus, which extends from the central fovea to more peripheral regions and covers a small section of polar angles (**Figure 6C**, *central*

http://dx.doi.org/10.5772/64562

inset). This wedge stimulus revolves either counterclockwise or clockwise in discrete steps around the central fixation point, successively stimulating distinct polar angle representations of visual space [3]. Each voxel's preferred eccentricity representation is measured by an expanding ring stimulus, which expands in discrete even steps between the central fovea and the periphery of the visual field (**Figure 6B**, *central inset*). These functional data are represented as color-coded overlays on anatomical data that demark the voxel's preferred polar angle or eccentricity (**Figure 6B** and **C**). The accurate delineation of VFMs relies upon the measurement of these two, orthogonal dimensions—polar angle and eccentricity, which produce a unique mapping between a location in visual space and the preferred responses of the neurons within a single voxel in cortex. If only a single measurement is obtained (e.g., of only polar angle or only eccentricity), the representation in cortex could only be associated with a wide section of visual space and would not lead to the correct definition of VFM boundaries (**Figure 5**) [3].

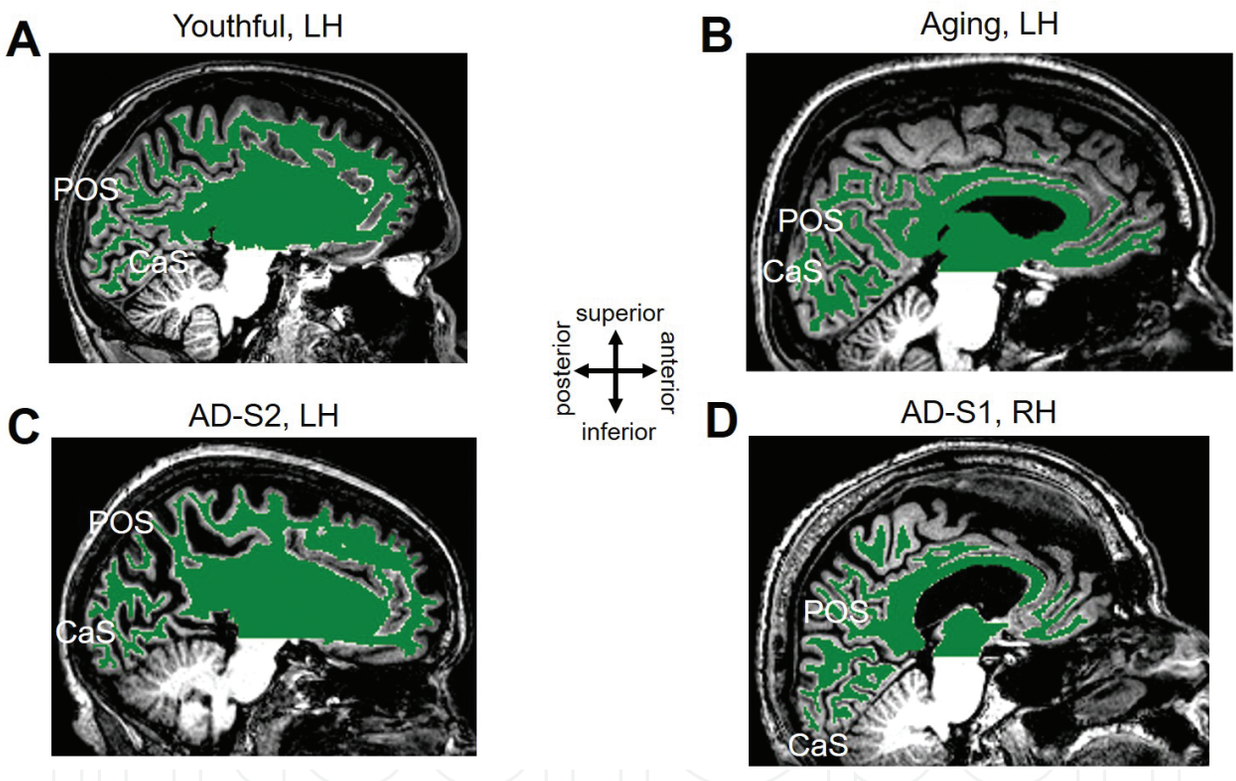

Figure 4. White/gray matter segmentation for young, healthy aging, and mild Alzheimer's disease subjects. Each panel is a T1-weighted 3D MPRAGE image showing a sagittal slice near the midline of the brain. Green-colored overlay represents white matter identified by an automated algorithm [104] and adjusted by hand-editing to minimize segmentation errors [1, 3, 92]. White regions below the green overlay represent unsegmented white matter within the cerebellum. Gray matter is shown as the gray regions along the surface of the green overlay and adjacent to the black cerebral spinal fluid (CSF; *black regions within the skull*). Middle inset displays approximate anatomical directions. CaS: calcarine sulcus; POS: parietal-occipital sulcus. **(A)** Left hemisphere of healthy young subject. **(B)** Left hemisphere of healthy aging subject. **(C)** Left hemisphere of a subject with mild Alzheimer's disease (AD-S2). **(D)** Right hemisphere of a second subject with mild Alzheimer's disease (AD-S1). Note how AD-S1's anatomy is relatively intact, but the visual field map measurements from this subject shown in **Figure 12** are perceptibly abnormal. Also compare the strikingly increased CSF-filled space in this T1 image of AD-S2 to the relatively normal visual field map organization for this subject in **Figure 12**. Data were adapted from [36, 37].

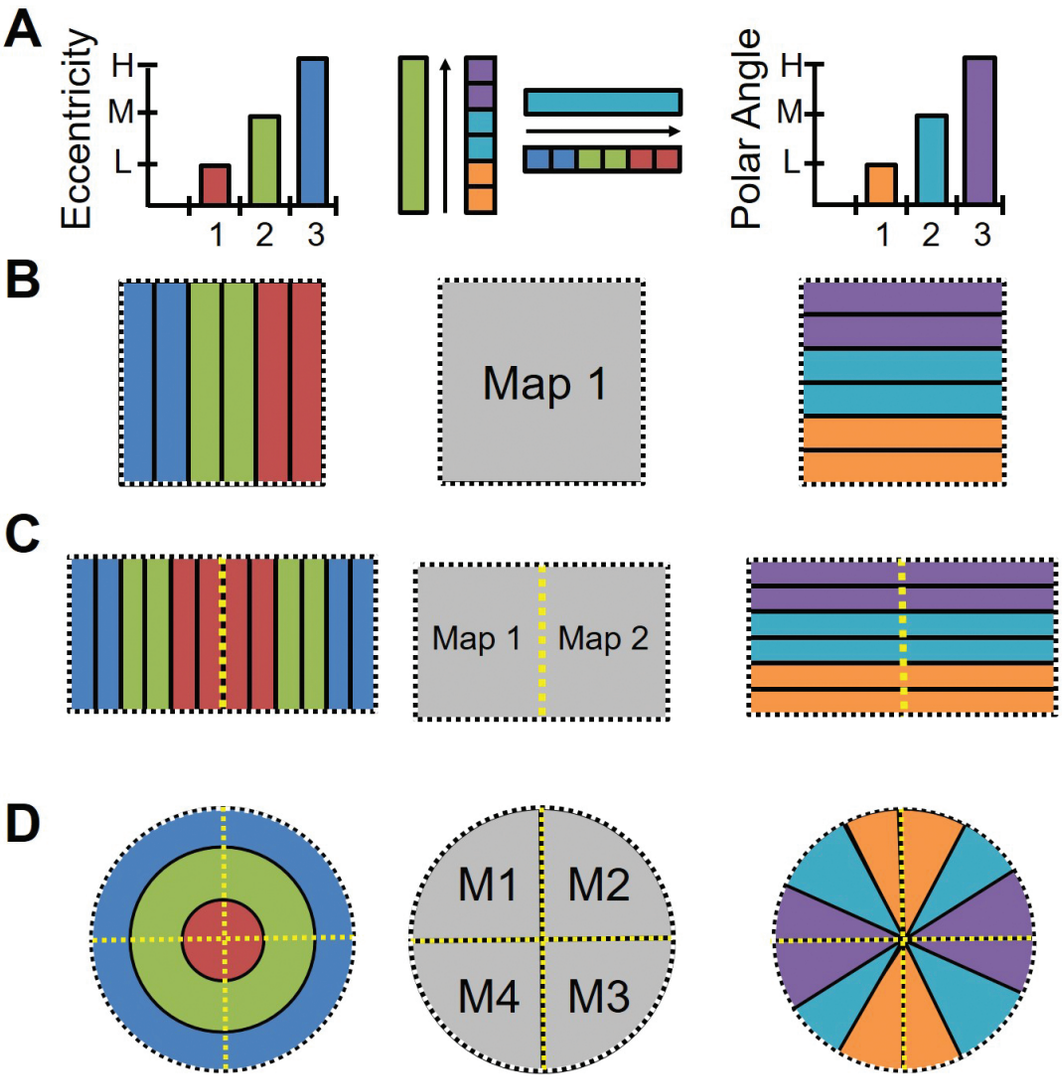

Figure 5. Two orthogonal gradients are required to define a cortical field map. (A)*Left:* The graph demonstrates measurements of three stimulus values—1: low (L, *red*); 2: medium (M, *green*); 3: high (H, *blue*)—for one sensory dimension (e.g., eccentricity). *Right:* The graph demonstrates measurements of three stimulus values—1: low (L, *orange*); 2: medium (M, *aqua*); 3: high (H, *purple*) for a second sensory dimension (e.g., polar angle). *Middle:* Schematic of the orthogonal gradients defining a cortical field map shows how measurements of the cortical representation of dimension 2 change along measurements of the representation of a single value of dimension 1, and vice versa. **(B)** Diagrams demonstrate how a single set of orthogonal gradients (one for each dimension) defines a single cortical field map. Black dotted lines demark the edge of the gradient representations. **(C)** Diagrams here demonstrate how a reversal in the dimension 1 gradient representations (*left*) divides up the single representation of the dimension 2 gradient (*right*) into two cortical field maps (*middle*). Yellow dotted lines demark a boundary defined by a gradient reversal, and black dotted lines again denote the edge of the gradient representations. A reversal in the dimension 2 gradient representations would similarly divide up a single representation of the dimension 1 gradient (*not shown*). **(D)** Cloverleaf cluster organization of multiple cortical field maps. *Left:* Schematic of an example macrostructural organization of dimension 1 (e.g., eccentricity) across a region of the cortical surface, with low (*red*) to medium (*green*) to high (*blue*) stimulus values represented in concentric circles. *Right:* Schematic of an example macrostructural organization of orthogonal dimension 2 (e.g., polar angle) across the same region of the cortical surface, with low (*orange*) to medium (*aqua*) to high (*purple*) stimulus values represented in wedges running "around the clock". *Middle:* Schematic shows the four cortical field maps defined by these orthogonal gradients and arranged in a cloverleaf cluster [3, 111–113]. Black dotted lines demark the edge of the gradient representations. Yellow dotted lines demark boundaries defined by a gradient reversal. For additional discussions, see [1, 3, 88].

http://dx.doi.org/10.5772/64562

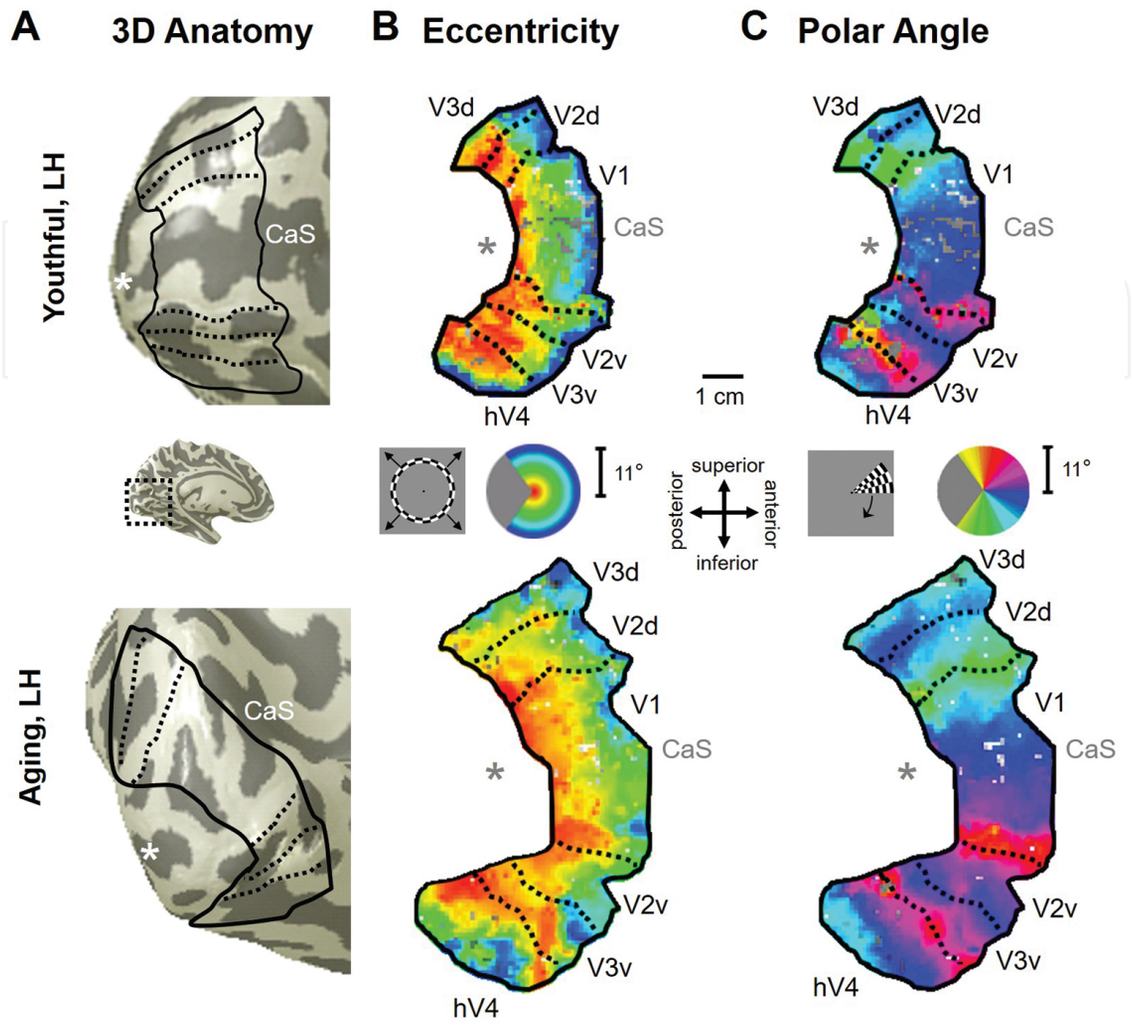

Figure 6. Visual field map measurements in healthy young and aging subjects. The images show example measurements of VFMs V1, V2, V3, and hV4 from a healthy young adult's left hemisphere (*top row*) and from a healthy aging adult's left hemisphere (*bottom row*). **(A)** Cortical locations of VFMs (black lines) are show on 3D renderings of each subject's left hemisphere. Central inset shows the approximate location of the cropped sections of the hemispheres. For cortical surfaces, dark gray represents sulci, and light gray represents gyri. "*" denotes the approximate location of the occipital pole; CaS: calcarine sulcus. **(B, C)** Flattened views of the cortical surfaces surrounding CaS are shown for the measurements of eccentricity **(B)** and polar angle **(C)** in each subject. The pseudocolor overlay on each flattened section of cortex signifies the location in visual space that creates the highest activity at each cortical position (see colored legend insets, *middle*). The wedge and ring stimuli each maximally spanned the central 11° radius of visual space. For simplicity, cortical representations are only shown for V1, V2, V3, and hV4—the VFMs of interest. Also note that functional data are only shown for voxels with a strong response at a coherence ≥0.20. Flattened renderings are scaled to the same size (see 1 cm scale bar, *middle inset*). Approximate anatomical directions for the flattened representations are shown in the central inset. Data were adapted from [36, 37].

The term "traveling wave" arises from the repeating pattern of cortical activity that is activated from one end of the VFM to the other along iso-angle or iso-eccentricity lines in response to these periodic stimuli (**Figure 2B**) [87, 91]. Thus, the time, or phase, of the peak modulation induced by the stimulus varies smoothly across the cortical surface. This phase defines the most effective stimulus eccentricity (i.e., ring) and polar angle (i.e., wedge) to activate that region of cortex, giving TWR its description as "phase-encoded retinotopy" (**Figure 2D**). This

paradigm only produces activity in regions that are retinotopically organized and is excellent for measuring early VFMs such as V1, V2, and V3.

In neuroimaging experiments, cortical activity driven by a particular stimulus is typically differentiated from unrelated activity and noise by setting well-defined statistical thresholds [94]. The statistical threshold for cortical activity arising from the TWR paradigm is commonly determined by coherence, which is equal to the amplitude of the blood-oxygen-level-dependent (BOLD) signal modulation at the frequency of stimulus presentation (e.g., six stimulus cycles per scan), divided by the square root of the power over all other frequencies except the first and second harmonics. Note that the activity must be correlated with the stimulus modulation frequency; unrelated activity at other frequencies is not included in the coherence measure. For each stimulus condition (e.g., wedge or ring), each voxel is independently assigned a coherence value, which denotes the strength of the BOLD response of that voxel for that particular stimulus (**Figure 2C**). Only voxels with a coherence above a chosen threshold —typically a coherence of 0.15–0.30—are further evaluated to determine the organization of cortical visual-spatial representations into specific VFMs [1, 3].

2.1.2. Population receptive field modeling

A newer method of measuring VFMs called population receptive field (pRF) modeling has been introduced not only for measurements of early visual cortex (e.g., V1–3), but also to improve measurements of the visual-spatial organization of higher-order regions that contain larger RFs (**Figures 1** and **3**) [92]. This model relies on the fact that the population of RFs in each voxel of retinotopically organized regions of cortex is expected to have similar preferred centers (i.e., location in visual space driving the peak neural responses) and sizes (i.e., the degrees of visual angle driving significant neural responses), allowing their combined pRF to be estimated as a single, two-dimensional Gaussian RF (**Figure 3B**). The pRF method does not require two distinct stimuli to measure orthogonal dimensions of visual space as in TWR, but can use any stimulus that systematically traverses the entire field of view. Most commonly in current measurements, this is a moving bar composed of the same checkerboard pattern with neutral gray blocks inserted at a nonstimulus frequency (**Figure 3C**). The neutral gray blocks allow for an estimation of a voxel's response to any visual stimulus versus just the preferred visual stimulus, which is necessary for the accurate measurement of pRF sizes.

For the first part of the analysis, the pRF model generates a database of many possible pRF centers and sizes within the field of view covered by the stimulus. The analysis then convolves the standard hemodynamic response function (HRF) with each of the possible pRFs (**Figure 3E**). Lastly, a least-squares fitting method is used to iteratively test the actual data collected against each of the possible pRFs for each voxel independently. The best-fit pRF position and size is then allocated as the pRF parameters for that voxel. As in TWR, further analysis is only performed on voxels with responses above a specific threshold of variance explained—which can be converted to coherence—as determined by the model are included for further analysis (for additional discussions, see [1, 3, 92]).

2.1.3. VFMs are defined using data from individual subjects

It is vital to correctly localize common functional areas across subjects in order to then study which specific computations are carried out by each area and how these functions change with damage and disease; however, the size of functional regions across the cortical surface varies significantly across individuals, complicating measurements across subject groups [14, 92, 98–102]. The surface area of primary visual cortex (V1) can differ across subjects by a factor of 3 or more; this variation in VFM size is independent of the total brain size [14]. Consequently, the position of each VFM with respect to the underlying structural anatomy varies across individuals. In addition, the amount of variation tends to increase from V1 to regions of visual cortex involved in higher-order computations (e.g., object recognition). Therefore, the common fMRI approach of averaging measurements across subjects does not work in the case of VFM data, as this approach will problematically blur the VFM boundaries to an unusable degree and may even destroy all traces of VFM organization in some regions [3]. Likewise, standardized brain-template coordinates (e.g., Talairach or Montreal Neurological Institute—MNI—coordinates) cannot be used to accurately estimate the position of any VFMs beyond area V1 in group-averaged or individual-subject data. Furthermore, issues like cortical degeneration introduce even greater variability into the match between cortical function and structure. The only accurate approach is to measure VFMs in individual subjects. Functional or structural measurements from each VFM—each region of interest (ROI) —can be obtained from individual subjects and then averaged across the subject group by VFM.

For analysis of such functional imaging data for individual subjects, several neuroimaging software packages are available. We use a signal-processing, Matlab-based software package called *mrVista*, which was originally developed by the Wandell lab at Stanford University and is now commonly available for neuroimaging analysis (http://white.stanford.edu/software/) [103, 104]. Using this software, each subject's cortical white matter is determined—"segmented"—in that subject's high-resolution anatomical scan, first with an automated algorithm and then by hand-editing to minimize errors for individual-subject analyses (**Figure 4**) [104]. Then a 3–4 mm layer of gray matter is automatically formed arising from the segmented white matter surface. Only data drawn from this identified gray matter are analyzed, in order to reduce extraneous measurements arising in the white matter or noise outside the head. The gray matter of the cortical sheet can then be visualized in three dimensions or as a flat sheet to allow analysis of functional activity within the sulci. For analysis of the functional data, linear trends are removed from the time series during preprocessing. Individual scans are inspected for motion artifacts; issues with motion between individual scans or across scan sessions can be corrected using mutual-information algorithms [105]; however, motion-correction algorithms should not be routinely applied if not needed, as they themselves may create artifacts. Once the preprocessed functional dataset is registered to the high-resolution anatomical scan, the VFM activity can be viewed along the cortical sheet to allow for optimal definition of VFM boundaries (e.g., **Figures 5** and **6**; for detailed discussions, see [1, 3, 88]). Importantly, we never apply spatial smoothing to the data, as smoothing will destroy key details of VFM organization, much like averaging data across subjects.

The description of a cortical "map" is frequently used nonspecifically for topographical gradients or other related cortical representations; however, it is advantageous for research into visual processing to explicitly define a "visual field map" in accordance with very exact criteria: (i) a VFM comprises two (or more) orthogonal, nonrepeating topographical representations of fundamental sensory dimensions (e.g., eccentricity and polar angle); (ii) each of these topographical representations must be organized as an generally contiguous, orderly gradient; (iii) each VFM should represent a substantial portion of sensory space (e.g., a hemifield of the visual field); and (iv) the general features of each VFM should be consistent across individuals (**Figure 5**) [1, 3, 13, 15, 88, 106–111]. For additional discussion, see *A Brief Primer on Cortical Field Mapping* in the supplemental material of [88].

2.2. Characteristics of V1, V2, V3, and hV4 in healthy young adults

Three VFMs known as V1, V2, and V3 occupy the medial wall of occipital cortex in humans and participate in the first stages of visual processing (for detailed reviews, see [1, 3]). Each represents a full hemifield of the opposite—i.e., contralateral—visual field in each hemisphere; the left hemisphere VFMs represent the right visual field, and vice versa (**Figure 6**).

V1 is very reliably located along the calcarine sulcus, bounded on either side by the unique split-hemifield representations of V2 and V3 on the cuneus and lingual gyri. V1, V2, and V3 each contain a representation of the center of visual space located at the occipital pole. Increasingly more peripheral representations form complete eccentricity gradients extending into more anteromedial cortex forming complete eccentricity gradients (**Figure 6A** and **B**; e.g., [1, 3, 13, 15, 91]). The position at which the central—i.e., foveal—representations of these three VFMs come together at the occipital pole is called the foveal confluence [114]. The boundaries between each map are delineated by reversals in polar angle gradients (**Figure 6A** and **C**). The polar angle gradient of V1 represents a contiguous hemifield of visual space. In contrast, the polar angle representations of V2 and V3 each consist of a split-hemifield representation (i.e., a quarterfield of visual space). The separate quarterfield sections are denoted by their positions ventral or dorsal to V1 (e.g., V2d, V2v, V3d, and V3v). For each of these three VFMs, the upper visual quarterfield is represented on the ventral surface, and the lower visual quarterfield is represented on the dorsal surface. The V2 and V3 quarterfields each meet at the fovea, but are otherwise separate [3]. Due to their relatively consistent anatomical locations and unique concentric organization, these three VFMs form the easiest landmarks to be identified in visual field mapping analyses [13–15, 87]. An additional VFM is adjacent to V3v along the ventral occipital surface: human V4, designated hV4 because of the unclear homology to macaque V4 [106]. The eccentricity representation of hV4 merges with the foveal confluence of V1, V2, and V3, and the polar angle representation moves smoothly from the boundary at the upper visual field representation of the V3v quarterfield into a full hemifield representation.

V1 is labeled as primary visual cortex, because it receives direct input from the retinal-thalamic pathway and is the first place along this pathway where information from the two eyes is combined [115]. In addition, V1 is an important site of initial basic calculations for such visual processing as orientation, color, and motion [116–120]. Beyond V1, perceptual calculations become more specialized, with V2 subserving relatively simple color and form perception and

V3 more selectively supporting motion processing [118, 119, 121–124]. hV4 serves as the next stage of the V1–V2 processing pathway with specialized neuronal populations for somewhat more complicated color and form visual perception [106, 125, 126]. Damage to part of the retina or V1 produces a complete loss of visual perception within the region normally processed by the damaged tissue in most cases [9], while damage to VFMs beyond V1 can produce more selective visual deficits like loss of color vision (i.e., achromatopsia; damage to hV4) or loss of motion perception (i.e., akinetopsia; damage to hMT+) [121, 127–131].

3. Specific changes occur in early visual cortex during otherwise healthy aging

In order to carefully evaluate alterations of visual cortex in the age-related neurodegenerative destruction of AD, we must investigate what changes occur across visual cortex during healthy aging [57, 132, 133]. To do so, studies have typically measured healthy visual aging in subjects over the age of 55 with no known age-related diseases or specific, clinically recognized deficits in vision. Major lesions along the retino-cortical visual pathways are not expected to occur in healthy aging, unlike in AD, but subtle retinal and cortical lesions as described below likely contribute to the variations in visual behavior associated with aging.

Lesion studies in young adult human subjects and animal models have outlined general expectations for changes in cortex that underlie the behavioral deficits arising from the loss of or alterations to the retina or visual pathways (**Figure 7**). Consider a retinal lesion that destroys function in the center of vision (i.e., the fovea). In this case, neurons with a pRF entirely within the cortical region to which the lesion projects (i.e., the lesion projection zone, LPZ) will be silenced, causing the cortical activity—and thus the corresponding BOLD signal—to drop to near zero and the distribution of the central eccentricity representation across the surface area of a VFM to shift to be more peripheral, as activity in the foveal representation would be lost (**Figure 7A** and **B**, *top row*). A second set of neurons would have RF centers located within the LPZ, but would have some of the spread of the pRF remain activated by still-healthy retinal regions. Here, the BOLD signal may drop somewhat but not completely, the surface area distribution would still shift toward the periphery, and the pRF centers of these neurons would also be measured as shifting toward the periphery (**Figure 7A** and **B**, *middle row*). Finally, a third set of neurons would have pRF centers outside of the LPZ, but would have some of the spread of the pRF still within the LPZ. Measurements of these neurons would likely show little drop in BOLD signal, a small shift of surface area distributions to the periphery, and also a small shift of pRF centers toward the periphery (**Figure 7A** and **B**, *bottom row*).

Anatomical and neuroimaging measurements from the few studies to date examining VFM changes in healthy aging have demonstrated several such changes in aging visual pathways that may contribute to such age-related behavioral changes as a decline in visual acuity, deficits in contrast sensitivity, and changes in color vision and visual-spatial attention. Next, we examine how such cortical changes may contribute to these healthy-aging behavioral deficits.

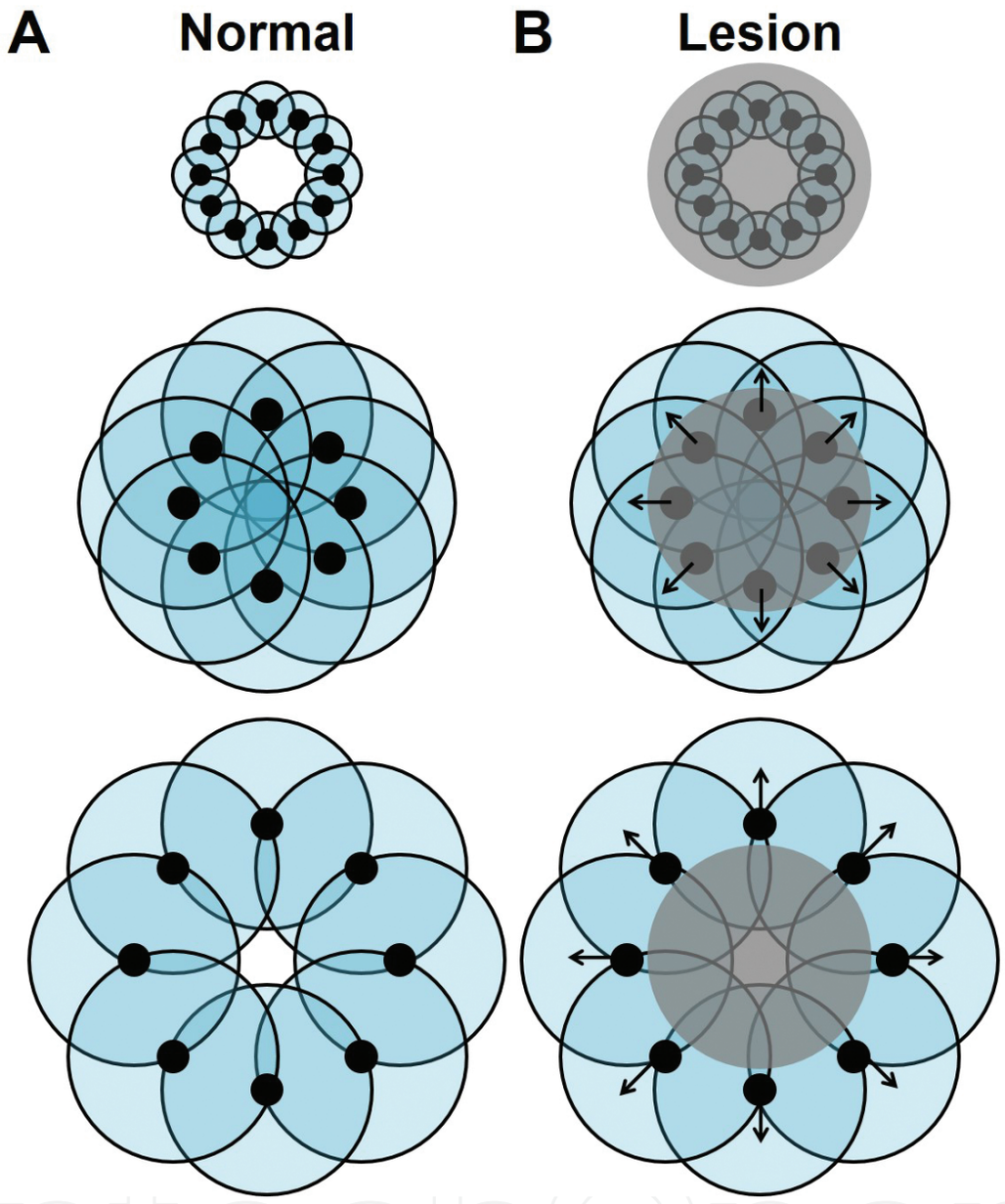

Figure 7. Schematic of the predicted effects of a retinal or cortical lesion on receptive field responses. (A) Solid black disks and the black-outlined teal circles around them indicate the preferred center and spread of a neuron's receptive field, respectively. Each row represents neurons with preferred centers at one specific eccentricity under normal conditions. **(B)** The gray-shaded regions indicate the lesion projection zone (LPZ) arising from retinal or cortical neuronal loss. The interaction of the LPZ with a neuron's receptive field is expected to shift the receptive field center more peripherally relative to normal conditions, as indicated by the black arrows. *Top:* RFs of these neurons are completely obscured by the LPZ. *Middle:* RFs of these neurons are partially obscured by the LPZ, and the RF centers fall within the LPZ. *Bottom:* RFs of these neurons are partially obscured by the LPZ, and the RF centers fall outside the LPZ. For additional discussions, see [8, 9, 12, 16].

3.1. Reductions in cortical activity

A change in cortical activity, whether from a change in peripheral inputs to a particular region (**Figure 7B**, *top row*) or from general changes in cortical responsivity with aging, is a likely

component of such aging deficits as a decrease in effective peripheral vision and problems with color discrimination. Given the increase in our knowledge of the role of certain cortical regions with specific behaviors, it is particularly interesting to examine changes in the level of activity of individual VFMs between healthy young adult and aging subjects.

3.1.1. Shrinkage of the useful field of view

Decrease in sensitivity across the visual field and a shrinkage of the useful field of view have been measured in behavioral studies of healthy aging subjects, with greater impairments in peripheral vision [28, 29, 38, 134]. The useful field of view is defined as the visual area in which information can be acquired while the eyes are held steady on a single fixation point. Within the useful field of view, a subject is able to detect, identify and discriminate visual stimuli without making an eye movement away from central fixation.

Measurements of visual search, in which the subject seeks a visual target (e.g., a single "T") hidden among distractors (e.g., many "L"s) demonstrated that there is a reduction as a function of increasing age in the size of the visual field used in the visual search task [38]. This reduction in the useful visual field size arises from a decrease in useful peripheral vision, but can be seen in healthy aging subjects without any clinical conditions affecting the optics of the eye. Although relative lens density increases with age and average pupil size is reduced, these changes do not account for the loss of useful peripheral vision or for the decrease in visual field sensitivity, which suggests that age-related visual field sensitivity changes are primarily due to neural losses rather than preretinal issues.

Evidence for how these changes may arise in cortex has been found with fMRI measurements of the BOLD signal modulation (measured as coherence) in early VFMs. In our recent study that used fMRI with pRF modeling to measure healthy aging VFM characteristics, the coherence of the peripheral 7–10° representation in V1 was found to be significantly lower in aging subjects than in youthful subjects (**Figure 8A**) [36, 37]. No significant differences in more peripheral regions of V2, V3, or hV4 were measured between subject groups (**Figure 8B–D**), so it is possible that the decrease in V1 alone—the primary visual cortex through which the majority of visual inputs pass—is sufficient to drive the behavioral changes. Due to the difficulty in setting up an fMRI paradigm to measure the visual periphery beyond 15–20°, no studies have yet investigated whether additional changes occur in this region across these VFMs.

Similarly, electrophysiology measurements of normally aging macaque monkeys have shown a significant decrease in the response-to-noise ratio and an increase in the neural-response variability in V1 and in the motion-selective medial temporal area (MT, also known as V5) in aging macaque monkeys [43]. These changes in cortical signals have been suggested to possibly arise from a degradation of inhibitory intra-cortical circuits in aging. With such degradations, the selectivity of particular neurons likely decreases, leading to greater activity arising from noise in a particular visual pathway and a consequent decrease in accurate signal-to-noise visual discrimination. In addition, anatomical studies of the visual pathway changes in normal aging humans demonstrate a decline in the retinal-nerve-fiber-layer thickness [46, 54] and a loss of retinal rod photoreceptors [49, 50, 53], both of which could cause a decrease in coherence

in peripheral V1 and subsequent VFMs as well as a reduction in the general visual field sensitivity.

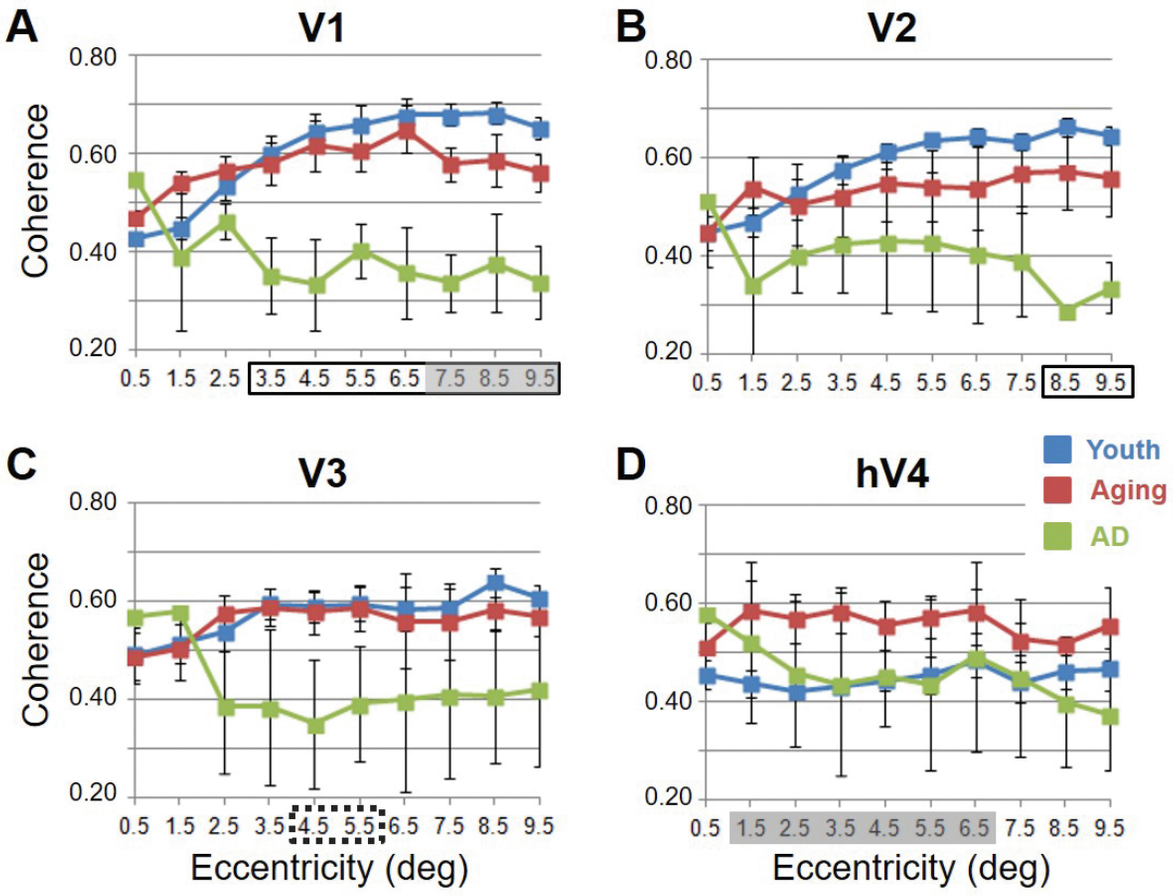

Figure 8. Average measurements of BOLD response in coherence for visual field maps in young, healthy aging, and mild Alzheimer's disease subjects. Blue lines represent data from healthy young subjects, red lines represent data from healthy aging subjects, and green lines represent data from AD subjects. Each line represents data measured in individual subjects and then averaged by iso-eccentricity band across hemispheres. Regions for each measurement shown to be significant are shown along the *x*-axis with shaded gray regions for comparisons between aging and youthful subjects and solid black lines for comparisons between AD and aging subjects. Dotted black lines represent regions shown to be marginally significant for comparisons between AD and aging subjects. Error bars indicate S.E.M. **(A)** V1; **(B)** V2; **(C)** V3; **(D)** hV4. Note the consistency for the youthful subjects and the somewhat greater variability for the healthy aging subjects. Also note both the decreased coherence and increased measurement variability for the AD subjects. Data were collected from [36, 37, 39].

3.1.2. Problems with color discrimination

Aging subjects frequently demonstrate losses in color discrimination—the ability to tell color hues apart—especially along the blue-yellow axis. While these issues can be partially attributed to changes in the aging lens [35] or to a loss of retinal S-cone (short wavelength) photoreceptors, which have a peak selectivity for shorter wave lengths of light [29, 30, 135], growing evidence points to additional concurrent neural changes underlying these deficits (e.g., [27, 37, 136]). For example, after corrections for preretinal losses, the decrease in the sensitivity of

S-cone pathways was found to be approximately 0.09 log units per decade in central vision, and these reductions became larger with measurements across the peripheral visual field to 30° [27]. M-cone (middle wavelength) and L-cone (long wavelength) pathways showed similar but not as severe age-related losses, with a decrease per decade of approximately 0.06–0.70 log units. Only some of this loss can be attributed to retinal changes, with the rest arising in central visual pathways.

Along these lines, fMRI measurements of cortical activity suggest that changes in the cortical color processing pathways may reflect issues with S-cone sensitivity and may further contribute to problems with color discrimination in normally aging subjects. Interestingly, our measurements of the BOLD coherence in hV4 demonstrated an increase in cortical activity over the central 1–7° of eccentricity in healthy aging relative to youthful subjects (**Figure 8D**) [37]. This coherence increase was consistent across all hemispheres in all subjects. It is possible that aging changes specific to the ventral visual color and form pathway involving V1, V2, and hV4 culminate in increased hV4 activity. In addition, although the total surface areas of V1–3 spanning the tested fields of view did not significantly change with age, the total surface area of hV4 was significantly smaller in the healthy aging subjects, perhaps due to losses in color pathway inputs (**Figure 9**) [36, 37, 39, 45]. Similar increases in occipital activity in healthy aging subjects in studies of visual working memory have been suggested to be a sign of a form of compensatory cognitive activity [55]; perhaps the increased hV4 activity in healthy aging similarly reflects a cognitive attempt to compensate for the reduced size of hV4 and/or for issues with color processing elsewhere in the visual pathways.

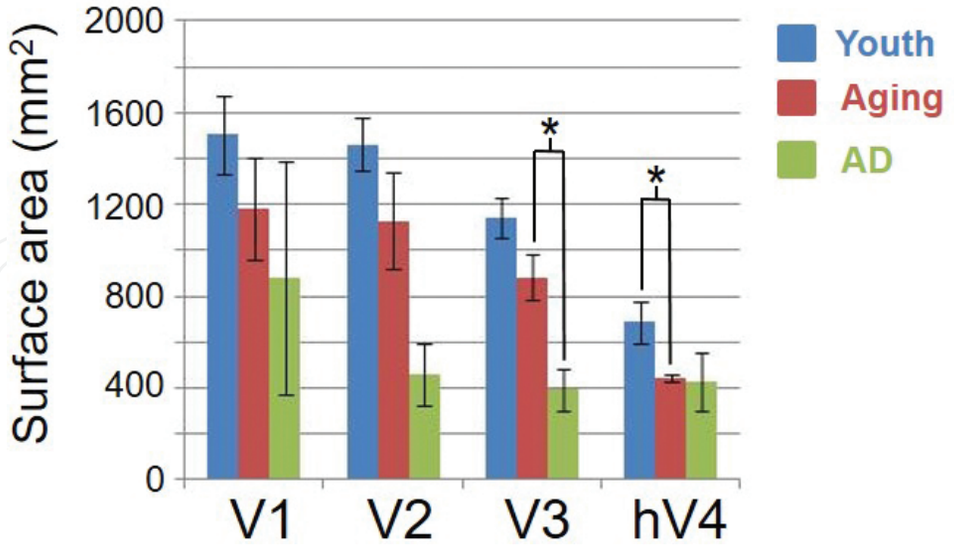

Figure 9. Total surface area measurements for visual field maps in young, healthy aging, and mild Alzheimer's disease subjects. Blue shading again indicates youthful subjects, red shading indicates normal aging subjects, and green shading indicates AD subjects. Total surface area in mm² for each visual field map was averaged across the individual subject measurements within in each group. "*" marks statistically significant differences ($p < 0.05$). Error bars indicate S.E.M. Data were collected from [36, 37].

3.2. Decreases in the cortical magnification of foveal representations

Cortical magnification is a common property of sensory systems that may arise from the increased cortical representation of a particular region of sensory space important for behavior. A change in the size of a specific part of a cortical representation between species or subject groups would suggest a related change in the functional properties of that region of cortex and possibly in behavior. For example, if the foveal representation of V1 is significantly reduced in extent for a particular patient group, then it is likely that there is a difference between those patients' central visual processing and that of healthy subjects with normally sized foveal representations (e.g., [8, 10, 12, 36, 37]).

Current measurements of cortical magnification usually consider only one dimension of visual space (e.g., position along eccentricity axis) and disregard the other dimension (e.g., position along polar angle axis) [14]. Thus, the cortical magnification factor as a function of position along the eccentricity axis does not reflect the magnification of representation along an iso-eccentricity line (i.e., across polar angles). We have recently altered such measurements to provide a measure that takes this "width" across polar angles into account by determining the surface-area-percent distributions for each VFM [3, 36, 37, 88, 111]. This is a measurement of what percentage of the total surface area of a VFM (spanning the tested field of view) is the surface area of the representation of a 1° band of eccentricity. As in cortical magnification, changes in the surface-area-percent distribution within a VFM can propose likely changes in function; for example, decreases in the foveal surface area may correlate with deficits in central vision (**Figure 7B**).

3.2.1. Decline in visual acuity

Our static visual acuity determines the smallest detail that we can distinguish in a stationary visual target. Such acuity has been shown to decline after 50 years of age, even in healthy aging subjects with good visual correction through glasses or contact lenses [24, 29, 41, 50, 137]. This loss in visual acuity is exacerbated by low contrast or low luminance in the visual scene [29]. As we rely on our central, foveal vision for our highest acuity, changes in foveal representations would be expected as part of a cortical contribution to this age-related decline in visual acuity.

Our pRF measurements of cortical surface area demonstrated just such a change, measuring a significant decrease in the foveal surface-area-percent distributions of early VFMs V1–hV4 for healthy aging subjects relative to young subjects (**Figure 10**, *red* and *blue lines*, respectively) [36, 37]. A second study by Crossland et al. [39] similarly measured a comparable decrease in the proportion of V1 representing the fovea, by comparing foveal eccentricity activations within polar angle measurements. These aging foveal-representation decreases are consistent with the decline in visual acuity seen normally in aging [24, 29, 41, 50, 137]. These measurements of foveal changes are unlikely to have arisen from unstable eye position, as Crossland et al. [39] demonstrated that aging has no effect on fixation stability, and models of improper fixation do not predict such results [12, 138]. Such a decrease in the size of the aging foveal representations across multiple early VFMs would be expected to lead to a loss in the resolution of cortical processing of visual information within the fovea, thus diminishing visual acuity.

http://dx.doi.org/10.5772/64562

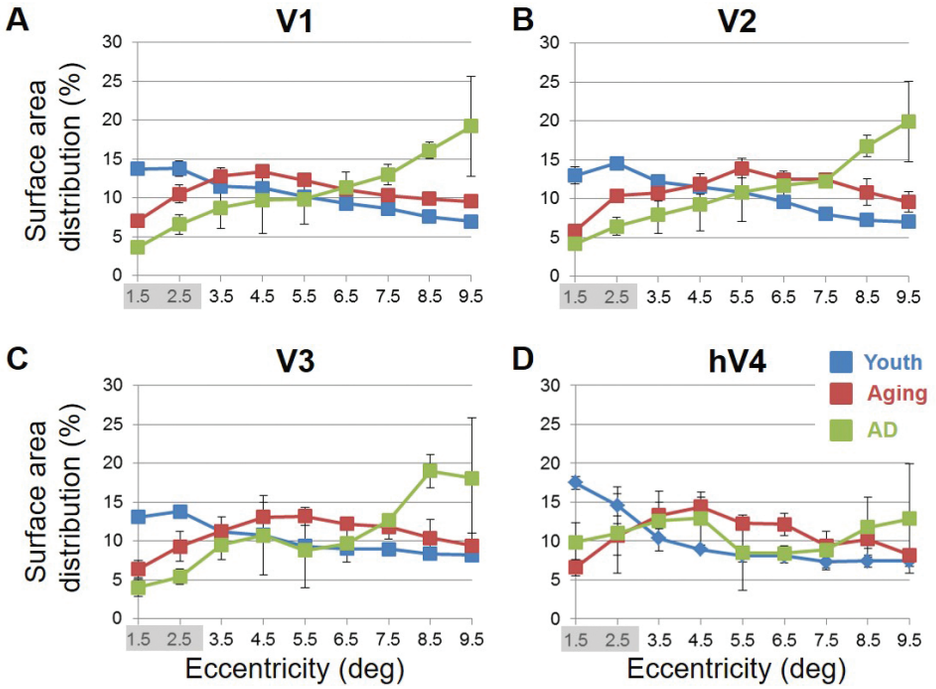

Figure 10. Surface area distribution as the percentage of total surface area. Graphs display average surface-area-percent-distribution measurements for visual field maps in young (*blue lines*), healthy aging (*red lines*), and AD (*green lines*) subjects. Each line represents data measured in individual subjects and then averaged by iso-eccentricity band across hemispheres. Regions for each measurement shown to be significantly different are shown with shaded gray regions for comparisons between aging and youthful subjects **(A)** V1; **(B)** V2; **(C)** V3; **(D)** hV4. Note the relatively increased foveal distribution in the youthful subjects, and the relatively increased peripheral distribution in AD subjects. Error bars indicate S.E.M. Data were collected from [36, 37].

3.2.2. Deficits in spatial and temporal contrast sensitivity

Spatial contrast is the difference in luminance (i.e., brightness) or color that makes an object within a visual scene distinguishable from the rest of the scene. Spatial contrast sensitivity, then, is a measure of a subject's ability to distinguish bright and dark aspects of a scene. This ability is a very important part of visual function, especially in situations of low light or glare (e.g., as in night driving), when the contrast between objects and their background is reduced. Spatial contrast sensitivity is commonly measured by a patient's ability to distinguish light and dark gratings, and age-related declines are most notable for gratings of intermediate and high spatial frequency [139, 140]. This problem cannot be eliminated by optimal lens correction [141, 142] or by elevated luminance [18, 141]. Along these lines, Elliot et al. [19, 33] demonstrated that the decrease in spatial contrast sensitivity at medium and high spatial frequencies with increasing age is mostly due to retinal and cortical changes rather than optical changes in the eye. The decreases in the surface-area-percent distributions of the V1–hV4 foveal representations in healthy aging compared with young adult subjects are likely to play a role in these spatial-contrast-sensitivity impairments, in addition to the decline in visual acuity described above (**Figure 10**) [36, 37, 39]. As the cortical territory devoted to central visual processing decreases, fewer neurons will be available to subserve behavioral discrimination of differences in spatial contrast.

The visual system also is sensitive to temporal contrast; temporal contrast sensitivity is a measure of the light-level difference (i.e., contrast modulation) required for an observer to be able discriminate a light source as flickering versus steady. Temporal contrast sensitivity is typically measured using a spatially uniform, randomly flickering stimulus. If the stimulus changes too slowly, an observer cannot detect the change, and if the stimulus changes too quickly, it is seen as a steady rather than flickering image. Similar to the problems with spatial contrast, aging subjects have decreased temporal contrast sensitivity at intermediate and high temporal frequencies [22, 25], as well as problems with motion discrimination [21, 32]. As human V1 and V3 have been implicated in motion processing [118, 143], the decreased foveal surface areas of aging V1 and V3 may similarly play a role in these temporal-contrast-sensitivity and motion-discrimination deficits (**Figure 10A** and **C**) [141].

3.2.3. Difficulties with visual-spatial attention

Visual-spatial attention is our ability to focus on a specific stimulus in our visual environment. When we look at a visual scene, our attention is drawn to a handful of locations that contain critical pieces of information. Normal visual processing relies on accurate and efficient use of visual-spatial attention, calibrated over a lifetime of visual experiences. Deficits in visual-spatial attention are associated with many neurological and neuropsychiatric disorders (e.g., hemispatial neglect [144], autism [145], schizophrenia [146]), and subtle problems with attention are thought to contribute to issues in healthy aging such as increased difficulty with driving [147, 148].

Measurements in macaque and human visual areas V1, V2, and V4 have demonstrated neural mechanisms in these VFMs possibly subserving selective visual-spatial attention [125, 149–151]. In humans, the significantly smaller surface areas of V2 from 1° to 7° and from 0° to 3° in V1 and hV4 in aging subjects likely denote issues in the processing of high acuity central vision in these regions. Such changes could then contribute to these deficits in visual-spatial attention, (**Figure 10A, B,** and **D**). In addition, the shrinkage of the useful field of view in aging described above may arise from issues correctly deploying visual-spatial attention to the periphery [28, 29, 31, 134].

3.3. Increases in the size of population receptive fields (pRFs)

As seen for cortical magnification, the receptive field sizes of sensory neurons suggest sensitivity to key aspects of sensory space. Smaller receptive fields can produce a higher resolution of sensory processing and suggest improved behavioral discrimination. For VFMs V1–hV4 in healthy subjects, the foveal representations are relatively magnified and also contain the smallest receptive fields [3, 14, 36, 92]. As inputs to visual areas are degraded, as from lesions to the retina or earlier visual pathways, these receptive fields tend to change in size (e.g., [8, 10, 12, 16, 152]). Changes can either be an increase in size, as, for example, normal lateral inhibition—which tends to refine and narrow receptive fields—is lost, or be a decrease in size, as inputs to that receptive field drop out (**Figure 7B**).

3.3.1. Enlargement of foveal pRFs likely contributes to many of the behavioral deficits associated with healthy aging

Further cortical changes that may contribute to the decreased visual acuity in normal aging include the differences in pRF sizes measured across the early VFMs of healthy aging subjects (**Figure 11**) [19, 26, 33, 36, 50]. Significant increases in pRF sizes are present in the foveal representations across V1, V2, V3, and hV4 from 0° to at least 3° of eccentricity [36, 37]. The ~2° foveal pRF size in the V1 of aging subjects is near that of the more peripheral pRF sizes (e.g., 5–7° of eccentricity) in young adults [36, 92]. Similarly, V2, V3, and hV4 of the healthy aging subjects contain foveal pRFs comparable in size to the pRF sizes of the more peripheral regions of these VFMs in healthy young subjects [37]. The increased foveal pRF sizes in these VFMs may reflect the decrease in visual acuity seen in healthy aging subjects. The decreased foveal surface area in the VFMs of aging subjects may drive these increases in pRF sizes as a compensatory mechanism, but we do not yet know whether such changes in pRF sizes arise directly within these VFMs during healthy aging or reflect other variations such as loss of retinal ganglion cells or alterations in feedback from higher-order VFMs.

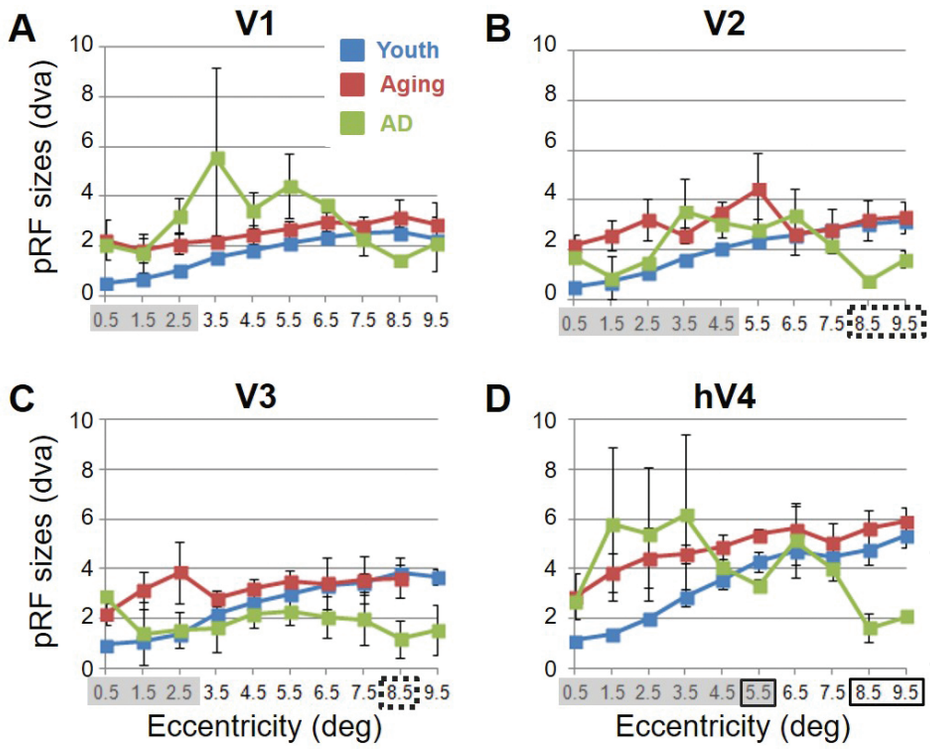

Figure 11. Average population receptive field size measurements for visual field maps in young, healthy aging, and mild Alzheimer's disease subjects. Average pRF radius in degrees of visual angle (dva) across each visual field map is shown for young (*blue lines*), healthy aging (*green lines*), and AD (*red lines*) subjects. Each line again represents data measured in individual subjects and then averaged by iso-eccentricity band across hemispheres. Regions for each measurement shown to be significantly different are shown with shaded gray regions for comparisons between aging and youthful subjects and solid black lines for comparisons between AD and aging subjects. Dotted black lines represent regions shown to be marginally significant for comparisons between AD and aging subjects **(A)** V1; **(B)** V2; **(C)** V3; **(D)** hV4. Note the generally increased pRF sizes and variability for measurements in aging and AD subjects relative to the youthful subjects. Data were collected from [36, 37].

In addition, the broadening of pRF sizes in the aging foveae of these four early VFMs is also consistent with the other behavioral deficits discussed in the sections above. Loss of resolution through these increased foveal pRF sizes likely underlies the decrease in spatial contrast sensitivity (**Figure 11**). The increased pRF sizes of aging V1 and V3 may similarly play a role in temporal-contrast-sensitivity and motion-discrimination deficits (**Figure 11A** and **C**). With respect to issues with color discrimination [27, 29, 30, 35], we have measured significant differences in pRF sizes in V2 and hV4 out to 5° and 6°, respectively, as well as foveal changes in V1 from 0° to 3° (**Figure 11A, B,** and **D**). It is possible that these greater regions of expanded pRFs in aging subjects are associated with aging changes specific to a ventral visual color and form pathway involving V1, V2, and hV4. Finally, V2 and hV4 both showed increases in pRF sizes across larger foveal and parafoveal regions (**Figure 11B** and **D**). These larger pRF sizes could reflect deficits in the proper tuning of visual-spatial attention and less ability to attend across the entire visual field.

4. Alzheimer's disease can present with additional changes in visual cortex

AD is characterized by progressive cognitive deficits including disturbances in memory, language, executive function, and vision [57, 84]. Somewhat surprisingly, it is not uncommon for visual deficits to be reported as one of the first symptoms of AD. However, despite many descriptions of visual symptoms in AD, only a very few studies have begun to examine the extent of changes in the organization, functionality, and connectivity of visual cortex that underlie these visual deficits.

4.1. Patterns of neurodegeneration in the visual cortex of AD patients

AD can present with a variety of visual symptoms across subjects, from lower-level deficits such as changes in visual acuity, contrast sensitivity, color discrimination, visual-spatial perception, and visual-processing speed [40, 73, 85, 132, 153, 154] to higher-level deficits such as problems in visual-spatial attention and in feature recognition of complex objects such as faces [40, 61, 63, 65, 69, 76, 78, 155, 156]. The neuropathology of AD results in gray matter lesions of varying density within regions of visual cortex [48, 57, 76, 84], and the visual symptoms could be attributed in part to a random pattern of neurodegeneration across regions of visual cortex [132]. However, there is also evidence for a more precise distribution of neurodegeneration in the AD visual pathways [48, 84], with some studies showing neurofibrillary tangles and neuritic senile plaques increasing steadily from primary to associative visual cortex and degenerative changes in both the retina ganglion cells and optic nerves [58, 59, 64, 66–68, 70]. The role that such changes may play in the visual symptoms of AD is discussed in the following sections.

Although AD is primarily a disorder of cortical gray matter, some studies have also shown a decreased density of the connections through the splenium of the corpus callosum, the region of the major interhemispheric white matter pathway that connects left and right visual cortex [47, 79, 157]. The changes in the white matter tracts in dementia may result from Wallerian

degeneration following retinal and cortical lesions or may be the product of a primary neuropathological process within the white matter itself. In the first case, we expect such white matter changes to reflect the behavioral deficits associated with the related gray matter or retinal lesion. In the latter, the direct loss of white matter connectivity may itself further contribute to these visual symptoms. Future studies tying functional MRI measurements of VFM organization and function together with diffusion tensor imaging (DTI) MR measurements of white matter tracts in the same subjects should help to clarify the presence and extent of each option in dementia with visual symptoms.

4.2. Visual deficits may arise in AD from both random and precise degenerative changes in cortex

fMRI measurements of cortical gray matter in AD subjects point to a combination of patterns of neurodegeneration, with some specific changes within cortical representations like VFMs seen consistently across subjects (e.g., **Figures 8–11**) in addition to variable alterations in gross

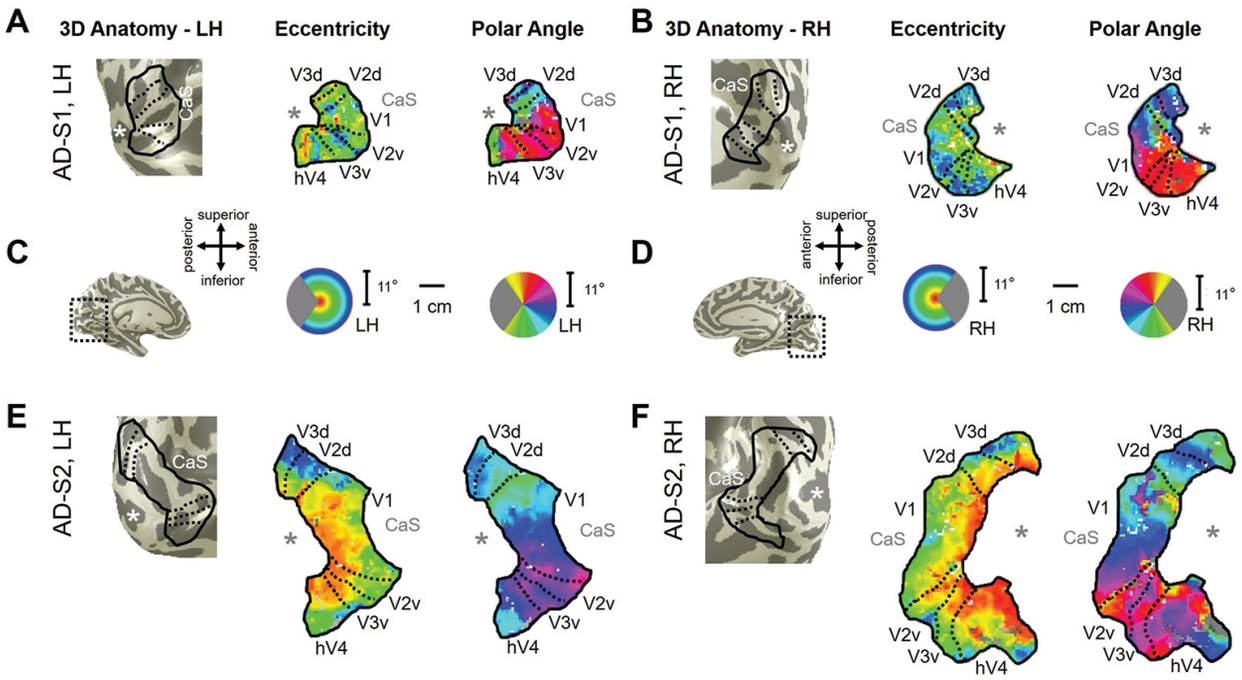

Figure 12. Visual field map measurements in mild Alzheimer's disease subjects. (A, B) Examples of VFMs V1, V2, V3, and hV4 are shown for the left **(A)** and right **(B)** hemispheres of a single subject with mild AD (AD-S1). For clarity, the visual responses are only shown for the VFMs of interest—V1, V2, V3, and hV4—and only voxels with a powerful response at a coherence ≥0.20 are colored. Note the visibly smaller size of these VFMs in this subject compared to those shown for young and healthy aging subjects in **Figure 6**. While the polar angle gradients still contain the expected representations of contralateral visual space with orderly reversals between VFMs, the eccentricity measurements, drawn from the same fMRI scans using the moving bar stimulus, are more disorganized. For cortical surfaces, dark gray represents sulci, and light gray represents gyri. "*" denotes the approximate location of the occipital pole. CaS: calcarine sulcus. **(C, D)** Images depict the full 3D cortical renderings, approximate anatomical orientations for each hemisphere, the color legends for the respective measurements, and the 1 cm scale bar. Note that all flattened hemispheres have been adjusted to the same scale; scale bar is duplicated for ease of comparison. **(E, F)** A second set of examples is shown for the left **(E)** and right **(F)** hemispheres from a second subject with mild AD (AD-S2). This AD subject displays more normal VFM sizes and foveal eccentricity representations, but also has visible changes in the peripheral eccentricity representations. Other details are as described in **Figure 6**. Data were collected from [37].

cortical organization (e.g., **Figure 12**). Measurements of both aspects of distributed neurodegeneration in the visual pathways can be useful in the diagnosis of AD in a specific individual and for understanding the progression this disease across cortex generally.

To date, the only neuroimaging study of VFM changes in AD patients that we are aware of is our Brewer and Barton (2014) study [36, 37], which used fMRI and pRF modeling to measure VFMs in a small number of patients with mild-to-moderate AD. Our results did not demonstrate simply a worsening of the deficits we measured in healthy aging subjects; rather, we observed both the visual deficits we found in healthy aging and additional changes in extrastriate VFMs (V2, V3, and hV4) unique to our AD subjects. Differences among our measurements of the hemispheres of each AD subject were likely primarily due to individual variations in the pattern and progression of neurodegeneration in each subject, revealed by detailed individual-subject data analysis. In addition, there were consistent patterns of changes across the cortical hemispheres that also likely reflected more uniform effects of AD on the visual pathways.

These measurements both demonstrated the feasibility of examining VFM changes in patients with dementia—despite the potentially difficult requirements of maintaining fixation and visual-spatial attention for several consecutive minutes—and emphasized the need for such detailed analyses in individual subjects for these types of investigations. Cortical changes seen consistently across AD patients may underlie the visual symptoms seen early in the disease [67] and may prove to be a useful tool for early and accurate diagnosis of AD. We review here some of the basic trends of VFM changes in AD patients, and, as above for healthy aging subjects, we suggest how these cortical changes may relate to specific deficits in visual behavior.

4.2.1. Declines in visual acuity and contrast sensitivity

Psychophysical studies have observed decreases in both visual acuity and contrast sensitivity in AD subjects beyond that expected for age-matched controls [71, 75]. In particular, psychophysical measures in AD patients showed a decrease in spatial contrast sensitivity for lower spatial frequencies than measured in the healthy aging population [40, 63]. Our measurements of significantly decreased BOLD coherence in regions of V1 and V2, with a marginally significant decrease in coherence in V3, could underlie these deficits (**Figure 8A–C**) [37]. Similarly, we found that the AD subjects significantly differed from healthy aging subjects in terms of total surface area of V3, with a general trend for decreased total surface area across V1–3 (**Figure 9**). While there were no significant differences in the surface area of V1 between healthy aging and AD subjects, the higher variability of these measurements highlights individual differences in neurodegenerative patterns in primary visual cortex as well as the need for additional studies of VFMs in a large number of AD subjects. On average, our AD subjects had no further decline in the surface-area-percent distribution of the foveal representation from 0° to 3° than that seen in the healthy aging subjects compared to youth (**Figure 10**). However, there was a trend for shifts from foveal to peripheral representations, which could point to a variable but important loss of central visual processing.

A striking feature of our AD measurements was the much-reduced total surface areas of V1–hV4 in one subject (AD-S1; **Figure 12A** and **B**). The shrunken VFMs additionally displayed very disorganized eccentricity representations with little foveal representation, likely due to an idiosyncratic pattern of neurodegeneration around the occipital pole. It is important to note that the polar angle representation, drawn from the same scan as the eccentricity representation, remained normal; thus the disorganization seen in the eccentricity representations cannot be simply attributed to a problem with that particular scan, but rather likely reflects alterations in visual function in this individual. Such a dramatic change in early VFM sizes would be expected to result in at least a significant decline in visual acuity and likely reflects changes in multiple aspects of visual processing; even so, the clinical examination of visual function in this subject reported no issues.

4.2.2. Deficiencies in color and form processing

Our measurements of VFM changes in AD were also consistent with the deficiencies in color and form processing frequently described in AD [73, 85, 153]. As suggested by Chan et al. [153], the degeneration of excitatory neurons in AD with the relative sparing of inhibitory interneurons in V1 may result in the color vision disorders reported by a subset of AD patients. This process could also drive the significant decrease we observed in pRF sizes in more peripheral hV4, a key region for color vision processing (**Figure 11D**). Patients with idiosyncratic foveal loss—as seen in our AD subject with greatly reduced VFM surface areas—might also present with these deficiencies in color and form processing.

4.2.3. Problems in the visual-spatial attentional network

Finally, the commonly reported changes in visual-spatial attention in AD patients may be related to the coherence changes we observed in V1 and V2 (**Figure 8**) [40, 63]. The marginally significant decreases in pRF sizes in the periphery of V2 and V3 and the significant pRF size decreases in the periphery of hV4 may also be involved in the deficiencies in the visual-spatial attentional network in AD and could contribute to the shrinkage of useful visual field that is often be even worse in AD patients than in healthy aging (**Figure 11B–D**) [72]. These cortical changes again may reflect degenerative disease in the retina and optic nerves or variations in feedback from higher-order VFMs [37]; some studies have shown that these regions contain more lesions in mild-to-moderate AD than V1 [48, 132]. In addition, V1, V2, and V4 both have been shown to play major roles in the visual-spatial attentional network, as described above [125, 149–151]. Future studies will be needed to examine whether similar changes in VFMs can be measured in the higher-order visual-spatial attention regions of parietal and frontal cortex (e.g., [158–161]).

4.3. These visual field map measurements may be able to improve the early diagnosis of specific types of dementia

Investigations into the early diagnosis of AD include such a wide range of methods as biochemical markers, cognitive testing, and structural and functional neuroimaging [47, 162,

163]. The ability to identify changes in cortical structure or function very early in the development of AD would increase the efficacy of treatments that stop the progression of the neurodegeneration before a significant amount of cortex is lost [62]. Neuroimaging measurements of VFM changes in patients with mild AD may provide an avenue for such early diagnosis, as these measurements can reveal subtle and highly detailed cortical changes using non-invasive fMRI [37]. In addition, these measurements in individual subjects also provide the opportunity to follow neurodegenerative changes in specific individuals over the course of their dementia progression (e.g., [9]). Further research into VFM characteristics in AD should include not only a larger population of AD patients, but also should examine the potential onset of visual symptoms in patients with mild cognitive impairment (MCI), which may provide an even earlier diagnostic tool [37, 55, 154, 164].

Disagreement also persists regarding the categorization of neurodegenerative symptoms into specific types of dementia. We do not yet have a complete understanding of how the different types of dementia—e.g., AD, PCA, DLB, etc.—vary with respect to the start of their associated neurodegenerative changes. Criteria have been outlined to differentiate AD from other dementias, but there still remains significant overlap across the symptoms associated with each dementia (e.g., [56, 78, 85, 86, 165]). The ability to distinguish a patient's particular type of dementia at an early time point in the disease may be vital for the identifying the correct treatment. Such comprehensive measurements of alterations in VFM characteristics as discussed here may assist in this early identification and diagnosis, as the onset and severity of changes in visual cortex are expected to follow patterns specific to each particular dementia [37].

5. Conclusion

Systematic changes in visual cortex likely occur as part of both the normal aging process and the pathophysiology of AD. A better understanding of the alteration of visual representations during healthy aging would both help reveal the effects of healthy aging on visual processing and enhance the use of age-matched controls in studies of visual symptoms in age-related diseases [57, 132]. Our hope is that such data will contribute to earlier and more definitive detection of these forms of dementia and a better understanding of the differences between AD and related dementias.

Acknowledgements

This work was supported in part by the National Institutes of Health Loan Repayment Program award #L30 EY019249 to A.A.B. and by the pilot grant to A.A.B. from the MIND Institute and Alzheimer's Disease Research Center at the University of California, Irvine, supported by the National Institutes of Health grant #AG16573.

Author details

Alyssa A. Brewer* and Brian Barton

*Address all correspondence to: aabrewer@uci.edu

Department of Cognitive Sciences, University of California, Irvine, CA, USA

References

[1] Wandell BA, Dumoulin SO, Brewer AA. Visual field maps in human cortex. Neuron. 2007;56(2):366–83. DOI: 10.1016/j.neuron.2007.10.012.

[2] Felleman DJ, Van Essen DC. Distributed hierarchical processing in the primate cerebral cortex. Cereb Cortex. 1991;1(1):1–47.

[3] Brewer AA, Barton B. Visual field map organization in human visual cortex. In: Molotchnikoff S, Rouat J, editors. Visual Cortex – Current Status and Perspectives. Rijeka, Croatia: InTech; 2012. pp. 29–60. DOI: 10.5772/51914.

[4] Mitchison G. Neuronal branching patterns and the economy of cortical wiring. Proc Biol Sci. 1991;245(1313):151–8. DOI: 10.1098/rspb.1991.0102.

[5] Chklovskii DB, Koulakov AA. Maps in the brain: what can we learn from them? Annu Rev Neurosci. 2004;27:369–92. DOI: 10.1146/annurev.neuro.27.070203.144226.

[6] Shapley R, Hawken M, Xing D. The dynamics of visual responses in the primary visual cortex. Prog Brain Res. 2007;165:21–32. DOI: 10.1016/S0079-6123(06)65003-6.

[7] Moradi F, Heeger DJ. Inter-ocular contrast normalization in human visual cortex. J Vis. 2009;9(3):13, 1–22. DOI: 10.1167/9.3.13.

[8] Baseler HA, Gouws A, Haak KV, Racey C, Crossland MD, Tufail A, et al. Large-scale remapping of visual cortex is absent in adult humans with macular degeneration. Nat Neurosci. 2011;14(5):649–55. DOI: 10.1038/nn.2793.

[9] Smirnakis SM, Brewer AA, Schmid MC, Tolias AS, Schuz A, Augath M, et al. Lack of long-term cortical reorganization after macaque retinal lesions. Nature. 2005;435(7040): 300–7. DOI: 10.1038/nature03495.

[10] Brewer AA, Barton B. Developmental plasticity: fMRI investigations into human visual cortex. In: Papageorgiou TD, Christopoulos G, Smirnakis S, editors. Advanced Brain Neuroimaging Topics in Health and Disease – Methods and Applications. Rijeka, Croatia: InTech; 2014. pp. 305–34. DOI: 10.5772/58256.

[11] Fine I, Wade AR, Brewer AA, May MG, Goodman DF, Boynton GM, et al. Long-term deprivation affects visual perception and cortex. Nat Neurosci. 2003;6(9):915–6. DOI: 10.1038/nn1102.

[12] Baseler HA, Brewer AA, Sharpe LT, Morland AB, Jagle H, Wandell BA. Reorganization of human cortical maps caused by inherited photoreceptor abnormalities. Nat Neurosci. 2002;5(4):364–70. DOI: 10.1038/nn817.

[13] DeYoe EA, Carman GJ, Bandettini P, Glickman S, Wieser J, Cox R, et al. Mapping striate and extrastriate visual areas in human cerebral cortex. Proc Natl Acad Sci USA. 1996;93:2382–6.

[14] Dougherty RF, Koch VM, Brewer AA, Fischer B, Modersitzki J, Wandell BA. Visual field representations and locations of visual areas V1/2/3 in human visual cortex. J Vis. 2003;3(10):586–98. DOI: 10:1167/3.10.1.

[15] Sereno MI, Dale AM, Reppas JB, Kwong KK, Belliveau JW, Brady TJ, et al. Borders of multiple visual areas in humans revealed by functional magnetic resonance imaging. Science. 1995;268(5212):889–93.

[16] Barton B, Brewer AA. fMRI of the rod scotoma elucidates cortical rod pathways and implications for lesion measurements. Proc Natl Acad Sci USA. 2015;112(16):5201–6. DOI: 10.1073/pnas.1423673112.

[17] Sloane ME, Owsley C, Alvarez SL. Aging, senile miosis and spatial contrast sensitivity at low luminance. Vision Res. 1988;28(11):1235–46.

[18] Sloane ME, Owsley C, Jackson CA. Aging and luminance-adaptation effects on spatial contrast sensitivity. J Opt Soc Am A. 1988;5(12):2181–90.

[19] Whitaker D, Elliott DB. Simulating age-related optical changes in the human eye. Docum Ophthalmol. 1992;82(4):307–16.

[20] Whitaker D, Elliott DB, MacVeigh D. Variations in hyperacuity performance with age. Ophthalmic Physiol Opt. 1992;12(1):29–32.

[21] Wojciechowski R, Trick GL, Steinman SB. Topography of the age-related decline in motion sensitivity. Optom Vis Sci. 1995;72(2):67–74.

[22] Wright CE, Drasdo N. The influence of age on the spatial and temporal contrast sensitivity function. Docum Ophthalmol. 1985;59(4):385–95.

[23] Wright CE, Williams DE, Drasdo N, Harding GF. The influence of age on the electroretinogram and visual evoked potential. Docum Ophthalmol. 1985;59(4):365–84.

[24] Pitts DG. The effects of aging on selected visual functions: dark adaptation, visual acuity, stereopsis, and brightness contrast. In: Sekuler R, Kline D, Dismukes K, editors. Aging and Human Visual Function. New York: Alan R. Liss; 1982. pp. 131–59.

[25] Mayer MJ, Kim CB, Svingos A, Glucs A. Foveal flicker sensitivity in healthy aging eyes. I. Compensating for pupil variation. J Opt Soc Am A. 1988;5(12):2201–9.

[26] Kline DW, Culham JC, Bartel P, Lynk L. Aging effects on vernier hyperacuity: a function of oscillation rate but not target contrast. Optom Vis Sci. 2001;78(9):676–82.

[27] Johnson CA, Adams AJ, Twelker JD, Quigg JM. Age-related changes in the central visual field for short-wavelength-sensitive pathways. J Opt Soc Am A. 1988;5(12):2131–9.

[28] Johnson CA, Adams AJ, Lewis RA. Evidence for a neural basis of age-related visual field loss in normal observers. Invest Ophthalmol Vis Sci. 1989;30(9):2056–64.

[29] Haegerstrom-Portnoy G, Schneck ME, Brabyn JA. Seeing into old age: vision function beyond acuity. Optom Vis Sci. 1999;76(3):141–58.

[30] Haegerstrom-Portnoy G, Hewlett SE, Barr SAN. S-cone loss with aging. In: Verriest G, editor. Colour vision deficiencies IX. The Hague: Junk Publisher; 1988. pp. 349–56.

[31] Haas A, Flammer J, Schneider U. Influence of age on the visual fields of normal subjects. Am J Ophthalmol. 1986;101(2):199–203.

[32] Gilmore GC, Wenk HE, Naylor LA, Stuve TA. Motion perception and aging. Psychol Aging. 1992;7(4):654–60.

[33] Elliott DB. Contrast sensitivity decline with ageing: a neural or optical phenomenon? Ophthal Physiolog Opt. 1987;7(4):415–9.

[34] Burton KB, Owsley C, Sloane ME. Aging and neural spatial contrast sensitivity: photopic vision. Vis Res. 1993;33(7):939–46.

[35] Bron AJ, Vrensen GF, Koretz J, Maraini G, Harding JJ. The ageing lens. Ophthalmologica. 2000;214(1):86–104.

[36] Brewer AA, Barton B. Effects of healthy aging on human primary visual cortex. Health. 2012;4(9A):695–702. DOI: 10.4236/health.2012.429109.

[37] Brewer AA, Barton B. Visual cortex in aging and Alzheimer's disease: changes in visual field maps and population receptive fields. Front Psychol. 2014;5:74. DOI: 10.3389/fpsyg.2014.00074.

[38] Ball KK, Beard BL, Roenker DL, Miller RL, Griggs DS. Age and visual search: expanding the useful field of view. J Opt Soc Am A. 1988;5(12):2210–9.

[39] Crossland MD, Morland AB, Feely MP, von dem Hagen E, Rubin GS. The effect of age and fixation instability on retinotopic mapping of primary visual cortex. Invest Ophthalmol Vis Sci. 2008;49(8):3734–9. DOI: 10.1167/iovs.07-1621.

[40] Thiyagesh SN, Farrow TF, Parks RW, Accosta-Mesa H, Young C, Wilkinson ID, et al. The neural basis of visuospatial perception in Alzheimer's disease and healthy elderly

comparison subjects: an fMRI study. Psychiatry Res. 2009;172(2):109–16. DOI: 10.1016/j.pscychresns.2008.11.002.

[41] Weale RA. Senile changes in visual acuity. Trans Ophthalmol Soc UK. 1975;95(1):36–8.

[42] Yang Y, Zhang J, Liang Z, Li G, Wang Y, Ma Y, et al. Aging affects the neural representation of speed in Macaque area MT. Cereb Cortex. 2009;19(9):1957–67. DOI: 10.1093/cercor/bhn221.

[43] Yang Y, Liang Z, Li G, Wang Y, Zhou Y. Aging affects response variability of V1 and MT neurons in rhesus monkeys. Brain Res. 2009;1274:21–7. DOI: 10.1016/j.brainres.2009.04.015.

[44] Raemaekers M, Vink M, van den Heuvel MP, Kahn RS, Ramsey NF. Effects of aging on BOLD fMRI during prosaccades and antisaccades. J Cogn Neurosci. 2006;18(4):594–603. DOI: 10.1162/jocn.2006.18.4.594.

[45] Raz N, Gunning-Dixon F, Head D, Rodrigue KM, Williamson A, Acker JD. Aging, sexual dimorphism, and hemispheric asymmetry of the cerebral cortex: replicability of regional differences in volume. Neurobiol Aging. 2004;25(3):377–96. DOI: 10.1016/S0197-4580(03)00118-0.

[46] Parikh RS, Parikh SR, Sekhar GC, Prabakaran S, Babu JG, Thomas R. Normal age-related decay of retinal nerve fiber layer thickness. Ophthalmology. 2007;114(5):921–6. DOI: 10.1016/j.ophtha.2007.01.023.

[47] Naggara O, Oppenheim C, Rieu D, Raoux N, Rodrigo S, Dalla Barba G, et al. Diffusion tensor imaging in early Alzheimer's disease. Psychiatry Res. 2006;146(3):243–9. DOI: 10.1016/j.pscychresns.2006.01.005.

[48] Lewis DA, Campbell MJ, Terry RD, Morrison JH. Laminar and regional distributions of neurofibrillary tangles and neuritic plaques in Alzheimer's disease: a quantitative study of visual and auditory cortices. J Neurosci. 1987;7(6):1799–808.

[49] Jackson GR, Owsley C, Curcio CA. Photoreceptor degeneration and dysfunction in aging and age-related maculopathy. Ageing Res Rev. 2002;1(3):381–96.

[50] Gao H, Hollyfield JG. Aging of the human retina. Differential loss of neurons and retinal pigment epithelial cells. Invest Ophthalmol Vis Sci. 1992;33(1):1–17.

[51] D'Esposito M, Zarahn E, Aguirre GK, Rypma B. The effect of normal aging on the coupling of neural activity to the bold hemodynamic response. Neuroimage. 1999;10(1):6–14. DOI: 10.1006/nimg.1999.0444.

[52] D'Esposito M, Deouell LY, Gazzaley A. Alterations in the BOLD fMRI signal with ageing and disease: a challenge for neuroimaging. Nat Rev Neurosci. 2003;4(11):863–72. DOI: 10.1038/nrn1246.

[53] Curcio CA, Millican CL, Allen KA, Kalina RE. Aging of the human photoreceptor mosaic: evidence for selective vulnerability of rods in central retina. Invest Ophthalmol Vis Sci. 1993;34(12):3278–96.

[54] Balazsi AG, Rootman J, Drance SM, Schulzer M, Douglas GR. The effect of age on the nerve fiber population of the human optic nerve. Am J Ophthalmol. 1984;97(6):760–6.

[55] Alichniewicz KK, Brunner F, Klunemann HH, Greenlee MW. Structural and functional neural correlates of visuospatial information processing in normal aging and amnestic mild cognitive impairment. Neurobiol Aging. 2012. DOI: 10.1016/j.neurobiolaging.2012.02.010.

[56] Armstrong RA, Lantos PL, Cairns NJ. Overlap between neurodegenerative disorders. Neuropathology. 2005;25(2):111–24.

[57] Yankner BA, Lu T, Loerch P. The aging brain. Ann Rev Pathol. 2008;3:41–66. DOI: 10.1146/annurev.pathmechdis.2.010506.092044.

[58] Danesh-Meyer HV, Birch H, Ku JY, Carroll S, Gamble G. Reduction of optic nerve fibers in patients with Alzheimer disease identified by laser imaging. Neurology. 2006;67(10):1852–4. DOI: 10.1212/01.wnl.0000244490.07925.8b.

[59] Berisha F, Feke GT, Trempe CL, McMeel JW, Schepens CL. Retinal abnormalities in early Alzheimer's disease. Invest Ophthalmol Vis Sci. 2007;48(5):2285–9. DOI: 10.1167/iovs.06-1029.

[60] Teipel SJ, Stahl R, Dietrich O, Schoenberg SO, Perneczky R, Bokde AL, et al. Multivariate network analysis of fiber tract integrity in Alzheimer's disease. Neuroimage. 2007;34(3):985–95. DOI: 10.1016/j.neuroimage.2006.07.047.

[61] van Rhijn SJ, Glosser G, de Vries JJ, Clark CM, Newberg AB, Alavi A. Visual processing impairments and decrements in regional brain activity in Alzheimer's disease. J Clin Exp Neuropsychol. 2004;26(1):11–23. DOI: 10.1076/jcen.26.1.11.23931.

[62] Rosen PN. Vision screening for Alzheimer's disease: prevention from an ophthalmologist's perspective (there is more to vision than meets the eye). Permanente J. 2004;8(1):15–21.

[63] Parasuraman R, Greenwood PM, Haxby JV, Grady CL. Visuospatial attention in dementia of the Alzheimer type. Brain. 1992;115(Pt 3):711–33.

[64] Paquet C, Boissonnot M, Roger F, Dighiero P, Gil R, Hugon J. Abnormal retinal thickness in patients with mild cognitive impairment and Alzheimer's disease. Neurosci Lett. 2007;420(2):97–9. DOI: 10.1016/j.neulet.2007.02.090.

[65] Pache M, Smeets CH, Gasio PF, Savaskan E, Flammer J, Wirz-Justice A, et al. Colour vision deficiencies in Alzheimer's disease. Age Ageing. 2003;32(4):422–6.

[66] Katz B, Rimmer S, Iragui V, Katzman R. Abnormal pattern electroretinogram in Alzheimer's disease: evidence for retinal ganglion cell degeneration? Ann Neurol. 1989;26(2):221–5. DOI: 10.1002/ana.410260207.

[67] Katz B, Rimmer S. Ophthalmologic manifestations of Alzheimer's disease. Surv Ophthalmol. 1989;34(1):31–43.

[68] Iseri PK, Altinas O, Tokay T, Yuksel N. Relationship between cognitive impairment and retinal morphological and visual functional abnormalities in Alzheimer disease. J Neuroophthalmol. 2006;26(1):18–24. DOI: 10.1097/01.wno.0000204645.56873.26.

[69] Holroyd S, Shepherd ML. Alzheimer's disease: a review for the ophthalmologist. Surv Ophthalmol. 2001;45(6):516–24.

[70] Hinton DR, Sadun AA, Blanks JC, Miller CA. Optic-nerve degeneration in Alzheimer's disease. N Engl J Med. 1986;315(8):485–7. DOI: 10.1056/NEJM198608213150804.

[71] Gilmore GC, Whitehouse PJ. Contrast sensitivity in Alzheimer's disease: a 1-year longitudinal analysis. Optom Vis Sci. 1995;72(2):83–91.

[72] Duchek JM, Hunt L, Ball K, Buckles V, Morris JC. Attention and driving performance in Alzheimer's disease. J Gerontol B Psychol Sci Soc Sci. 1998;53(2):P130–41.

[73] Cronin-Golomb A, Sugiura R, Corkin S, Growdon JH. Incomplete achromatopsia in Alzheimer's disease. Neurobiol Aging. 1993;14(5):471–7.

[74] Cronin-Golomb A, Rizzo JF, Corkin S, Growdon JH. Visual function in Alzheimer's disease and normal aging. Ann NY Acad Sci. 1991;640:28–35.

[75] Cronin-Golomb A, Corkin S, Rizzo JF, Cohen J, Growdon JH, Banks KS. Visual dysfunction in Alzheimer's disease: relation to normal aging. Ann Neurol. 1991;29(1): 41–52. DOI: 10.1002/ana.410290110.

[76] Giannakopoulos P, Gold G, Duc M, Michel JP, Hof PR, Bouras C. Neuroanatomic correlates of visual agnosia in Alzheimer's disease: a clinicopathologic study. Neurology. 1999;52(1):71–7.

[77] Giannakopoulos P, Gold G, Duc M, Michel JP, Hof PR, Bouras C. Neural substrates of spatial and temporal disorientation in Alzheimer's disease. Acta Neuropathol. 2000;100(2):189–95.

[78] Tang-Wai DF, Graff-Radford NR, Boeve BF, Dickson DW, Parisi JE, Crook R, et al. Clinical, genetic, and neuropathologic characteristics of posterior cortical atrophy. Neurology. 2004;63(7):1168–74.

[79] Yoshida T, Shiga K, Yoshikawa K, Yamada K, Nakagawa M. White matter loss in the splenium of the corpus callosum in a case of posterior cortical atrophy: a diffusion tensor imaging study. Eur Neurol. 2004;52(2):77–81. DOI: 10.1159/000079750.

[80] Whitwell JL, Jack CR, Jr., Kantarci K, Weigand SD, Boeve BF, Knopman DS, et al. Imaging correlates of posterior cortical atrophy. Neurobiol Aging. 2007;28(7):1051–61. DOI: 10.1016/j.neurobiolaging.2006.05.026.

[81] Schmidtke K, Hull M, Talazko J. Posterior cortical atrophy: variant of Alzheimer's disease? A case series with PET findings. J Neurol. 2005;252(1):27–35. DOI: 10.1007/s00415-005-0594-5.

[82] Mendez MF, Ghajarania M, Perryman KM. Posterior cortical atrophy: clinical characteristics and differences compared to Alzheimer's disease. Dement Geriatr Cogn Disord. 2002;14(1):33–40.

[83] Charles RF, Hillis AE. Posterior cortical atrophy: clinical presentation and cognitive deficits compared to Alzheimer's disease. Behav Neurol. 2005;16(1):15–23.

[84] Black SE. Focal cortical atrophy syndromes. Brain Cogn. 1996;31(2):188–229. DOI: 10.1006/brcg.1996.0042.

[85] Sauer J, ffytche DH, Ballard C, Brown RG, Howard R. Differences between Alzheimer's disease and dementia with Lewy bodies: an fMRI study of task-related brain activity. Brain. 2006;129(Pt 7):1780–8. DOI: 10.1093/brain/awl102.

[86] Harding AJ, Broe GA, Halliday GM. Visual hallucinations in Lewy body disease relate to Lewy bodies in the temporal lobe. Brain. 2002;125(Pt 2):391–403.

[87] Engel SA, Rumelhart DE, Wandell BA, Lee AT, Glover GH, Chichilnisky EJ, et al. fMRI of human visual cortex. Nature. 1994;369(6481):525. DOI: 10.1038/369525a0.

[88] Brewer AA, Barton B. Maps of auditory cortex. Annu Rev Neurosci. 2016;39(1):385–407. DOI: 10.1146/annurev-neuro-070815-014045.

[89] Bartels A, Zeki S. The theory of multistage integration in the visual brain. Proc R Soc Lond B Biol Sci. 1998;265(1412):2327–32. DOI: 10.1098/rspb.1998.0579.

[90] VanEssen D. Organization of visual areas in Macaque and human cerebral cortex. In: Chalupa L, Werner J, editors. The Visual Neurosciences. Boston: Bradford Books; 2003. pp. 507–21.

[91] Engel SA, Glover GH, Wandell BA. Retinotopic organization in human visual cortex and the spatial precision of functional MRI. Cereb Cortex. 1997;7(2):181–92.

[92] Dumoulin SO, Wandell BA. Population receptive field estimates in human visual cortex. Neuroimage. 2008;39(2):647–60. DOI: 10.1016/j.neuroimage.2007.09.034.

[93] Wandell BA, Winawer J. Imaging retinotopic maps in the human brain. Vision Res. 2011;51(7):718–37. DOI: 10.1016/j.visres.2010.08.004.

[94] Boynton GM, Engel SA, Glover GH, Heeger DJ. Linear systems analysis of functional magnetic resonance imaging in human V1. J Neurosci. 1996;16(13):4207–21.

[95] Birn RM, Saad ZS, Bandettini PA. Spatial heterogeneity of the nonlinear dynamics in the FMRI BOLD response. Neuroimage. 2001;14(4):817–26. DOI: 10.1006/nimg.2001.0873.

[96] Hansen KA, David SV, Gallant JL. Parametric reverse correlation reveals spatial linearity of retinotopic human V1 BOLD response. Neuroimage. 2004;23(1):233–41. DOI: 10.1016/j.neuroimage.2004.05.012.

[97] Friston KJ, Fletcher P, Josephs O, Holmes A, Rugg MD, Turner R. Event-related fMRI: characterizing differential responses. Neuroimage. 1998;7(1):30–40. DOI: 10.1006/nimg.1997.0306.

[98] Leonard CM, Puranik C, Kuldau JM, Lombardino LJ. Normal variation in the frequency and location of human auditory cortex landmarks. Heschl's gyrus: where is it? Cereb Cortex. 1998;8(5):397–406.

[99] Rademacher J, Caviness VS, Jr., Steinmetz H, Galaburda AM. Topographical variation of the human primary cortices: implications for neuroimaging, brain mapping, and neurobiology. Cereb Cortex. 1993;3(4):313–29.

[100] Rademacher J, Morosan P, Schormann T, Schleicher A, Werner C, Freund HJ, et al. Probabilistic mapping and volume measurement of human primary auditory cortex. Neuroimage. 2001;13(4):669–83. DOI: 10.1006/nimg.2000.0714.

[101] Amunts K, Schleicher A, Burgel U, Mohlberg H, Uylings HB, Zilles K. Broca's region revisited: cytoarchitecture and intersubject variability. J Comp Neurol. 1999;412(2):319–41.

[102] Clarke S, Morosan P. Architecture, connectivity, and transmitter receptors of human auditory cortex. In: Poeppel D, Overath T, Popper A, Richard R, editors. The Human Auditory Cortex. New York: Springer; 2012. pp. 11–38.

[103] Wandell BA, Chial S, Backus BT. Visualization and measurement of the cortical surface. J Cogn Neurosci. 2000;12(5):739–52.

[104] Teo PC, Sapiro G, Wandell BA. Creating connected representations of cortical gray matter for functional MRI visualization. IEEE Trans Med Imaging. 1997;16(6):852–63. DOI: 10.1109/42.650881.

[105] Nestares O, Heeger DJ. Robust multiresolution alignment of MRI brain volumes. Magn Reson Med. 2000;43(5):705–15.

[106] Brewer AA, Liu J, Wade AR, Wandell BA. Visual field maps and stimulus selectivity in human ventral occipital cortex. Nat Neurosci. 2005;8(8):1102–9. DOI: 10.1038/nn1507.

[107] Van Essen DC. Organization of visual areas in Macaque and human cerebral cortex. In: Chalupa LM, Werner JS, editors. The Visual Neurosciences. Boston: Bradford Books; 2003. pp. 507–21.

[108] Zeki S. Improbable areas in the visual brain. Trends Neurosci. 2003;26(1):23–6.

[109] Press WA, Brewer AA, Dougherty RF, Wade AR, Wandell BA. Visual areas and spatial summation in human visual cortex. Vision Res. 2001;41(10–11):1321–32.

[110] Baumann S, Griffiths TD, Sun L, Petkov CI, Thiele A, Rees A. Orthogonal representation of sound dimensions in the primate midbrain. Nat Neurosci. 2011;14(4):423–5. DOI: 10.1038/nn.2771.

[111] Barton B, Venezia JH, Saberi K, Hickok G, Brewer AA. Orthogonal acoustic dimensions define auditory field maps in human cortex. Proc Natl Acad Sci USA. 2012;109(50): 20738–43. DOI: 10.1073/pnas.1213381109.

[112] Kolster H, Mandeville JB, Arsenault JT, Ekstrom LB, Wald LL, Vanduffel W. Visual field map clusters in macaque extrastriate visual cortex. J Neurosci. 2009;29(21):7031–9. DOI: 10.1523/JNEUROSCI.0518-09.2009.

[113] Kolster H, Peeters R, Orban GA. The retinotopic organization of the human middle temporal area MT/V5 and its cortical neighbors. J Neurosci. 2010;30(29):9801–20. DOI: 10.1523/JNEUROSCI.2069-10.2010.

[114] Schira MM, Tyler CW, Breakspear M, Spehar B. The foveal confluence in human visual cortex. J Neurosci. 2009;29(28):9050–8. DOI: 10.1523/JNEUROSCI.1760-09.2009.

[115] Adams DL, Sincich LC, Horton JC. Complete pattern of ocular dominance columns in human primary visual cortex. J Neurosci. 2007;27(39):10391–403. DOI: 10.1523/JNEUROSCI.2923-07.2007.

[116] Bartfeld E, Grinvald A. Relationships between orientation-preference pinwheels, cytochrome oxidase blobs, and ocular-dominance columns in primate striate cortex. Proc Natl Acad Sci USA. 1992;89(24):11905–9.

[117] Livingstone MS, Hubel DH. Anatomy and physiology of a color system in the primate visual cortex. J Neurosci. 1984;4(1):309–56.

[118] Smith AT, Greenlee MW, Singh KD, Kraemer FM, Hennig J. The processing of first- and second-order motion in human visual cortex assessed by functional magnetic resonance imaging (fMRI). J Neurosci. 1998;18(10):3816–30.

[119] Zeki S. The distribution of wavelength and orientation selective cells in different areas of monkey visual cortex. Proc R Soc Lond B Biol Sci. 1983;217(1209):449–70.

[120] Zeki S. The relationship between wavelength and color studied in single cells of monkey striate cortex. Prog Brain Res. 1983;58:219–27. DOI: 10.1016/S0079-6123(08)60023-0.

[121] Bartels A, Zeki S. The architecture of the colour centre in the human visual brain: new results and a review. Eur J Neurosci. 2000;12(1):172–93.

[122] Zeki S, Watson JD, Lueck CJ, Friston KJ, Kennard C, Frackowiak RS. A direct demonstration of functional specialization in human visual cortex. J Neurosci. 1991;11(3):641–9.

[123] Amano K, Wandell BA, Dumoulin SO. Visual field maps, population receptive field sizes, and visual field coverage in the human MT+ complex. J Neurophysiol. 2009;102(5):2704–18. DOI: 10.1152/jn.00102.2009.

[124] Huk AC, Dougherty RF, Heeger DJ. Retinotopy and functional subdivision of human areas MT and MST. J Neurosci. 2002;22(16):7195–205.

[125] Gallant JL, Shoup RE, Mazer JA. A human extrastriate area functionally homologous to macaque V4. Neuron. 2000;27(2):227–35.

[126] Wade AR, Brewer AA, Rieger JW, Wandell BA. Functional measurements of human ventral occipital cortex: retinotopy and colour. Philos Trans R Soc Lond B Biol Sci. 2002;357(1424):963–73. DOI: 10.1098/rstb.2002.1108.

[127] Zeki S, Bartels A. The autonomy of the visual systems and the modularity of conscious vision. Philos Trans R Soc Lond B Biol Sci. 1998;353(1377):1911–4. DOI: 10.1098/rstb.1998.0343.

[128] Zeki S. A century of cerebral achromatopsia. Brain. 1990;113(Pt 6):1721–77.

[129] Meadows JC. Disturbed perception of colours associated with localized cerebral lesions. Brain. 1974;97(4):615–32.

[130] Vaina LM. Functional segregation of color and motion processing in the human visual cortex: clinical evidence. Cereb Cortex. 1994;4(5):555–72.

[131] Beckers G, Homberg V. Cerebral visual motion blindness: transitory akinetopsia induced by transcranial magnetic stimulation of human area V5. Philos Trans R Soc Lond B Biol Sci. 1992;249(1325):173–8. DOI: 10.1098/rspb.1992.0100.

[132] Jackson GR, Owsley C. Visual dysfunction, neurodegenerative diseases, and aging. Neurol Clin. 2003;21(3):709–28.

[133] Raz N, Rodrigue KM, Head D, Kennedy KM, Acker JD. Differential aging of the medial temporal lobe: a study of a five-year change. Neurology. 2004;62(3):433–8.

[134] Ball K, Owsley C. The useful field of view test: a new technique for evaluating age-related declines in visual function. J Am Optom Assoc. 1993;64(1):71–9.

[135] Werner JS, Steele VG. Sensitivity of human foveal color mechanisms throughout the life span. J Opt Soc Am A. 1988;5(12):2122–30.

[136] Schefrin BE, Werner JS, Plach M, Utlaut N, Switkes E. Sites of age-related sensitivity loss in a short-wave cone pathway. J Opt Soc Am A. 1992;9(3):355–63.

[137] Elliott DB, Yang KC, Whitaker D. Visual acuity changes throughout adulthood in normal, healthy eyes: seeing beyond 6/6. Optom Vis Sci. 1995;72(3):186–91.

[138] Levin N, Dumoulin SO, Winawer J, Dougherty RF, Wandell BA. Cortical maps and white matter tracts following long period of visual deprivation and retinal image restoration. Neuron. 2010;65(1):21–31. DOI: 10.1016/j.neuron.2009.12.006.

[139] Elliott D, Whitaker D, MacVeigh D. Neural contribution to spatiotemporal contrast sensitivity decline in healthy ageing eyes. Vis Res. 1990;30(4):541–7.

[140] Kline DW, Schieber F, Abusamra LC, Coyne AC. Age, the eye, and the visual channels: contrast sensitivity and response speed. J Gerontol. 1983;38(2):211–6.

[141] Owsley C, Sekuler R, Siemsen D. Contrast sensitivity throughout adulthood. Vis Res. 1983;23(7):689–99.

[142] Scialfa CT, Adams EM, Giovanetto M. Reliability of the Vistech Contrast Test System in a life-span adult sample. Optom Vis Sci. 1991;68(4):270–4.

[143] McKeefry DJ, Watson JD, Frackowiak RS, Fong K, Zeki S. The activity in human areas V1/V2, V3, and V5 during the perception of coherent and incoherent motion. Neuroimage. 1997;5(1):1–12. DOI: 10.1006/nimg.1996.0246.

[144] Hillis AE, Newhart M, Heidler J, Barker PB, Herskovits EH, Degaonkar M. Anatomy of spatial attention: insights from perfusion imaging and hemispatial neglect in acute stroke. J Neurosci. 2005;25(12):3161–7. DOI: 10.1523/JNEUROSCI.4468-04.2005.

[145] Mundy P, Sullivan L, Mastergeorge AM. A parallel and distributed-processing model of joint attention, social cognition and autism. Autism Res. 2009;2(1):2–21. DOI: 10.1002/aur.61.

[146] Maruff P, Hay D, Malone V, Currie J. Asymmetries in the covert orienting of visual spatial attention in schizophrenia. Neuropsychologia. 1995;33(10):1205–23.

[147] Ball K, Owsley C, Sloane ME, Roenker DL, Bruni JR. Visual attention problems as a predictor of vehicle crashes in older drivers. Invest Ophthalmol Vis Sci. 1993;34(11):3110–23.

[148] Owsley C, Ball K. Assessing visual function in the older driver. Clin Geriatr Med. 1993;9(2):389–401.

[149] Luck SJ, Chelazzi L, Hillyard SA, Desimone R. Neural mechanisms of spatial selective attention in areas V1, V2, and V4 of macaque visual cortex. J Neurophysiol. 1997;77(1):24–42.

[150] Reynolds JH, Pasternak T, Desimone R. Attention increases sensitivity of V4 neurons. Neuron. 2000;26(3):703–14.

[151] Serences JT, Yantis S. Selective visual attention and perceptual coherence. Trends Cogn Sci. 2006;10(1):38–45. DOI: 10.1016/j.tics.2005.11.008.

[152] Haak KV, Cornelissen FW, Morland AB. Population receptive field dynamics in human visual cortex. PLoS One. 2012;7(5):e37686. DOI: 10.1371/journal.pone.0037686.

[153] Chan D, Crutch SJ, Warrington EK. A disorder of colour perception associated with abnormal colour after-images: a defect of the primary visual cortex. J Neurol, Neurosurg Psych. 2001;71(4):515–7.

[154] Mapstone M, Steffenella TM, Duffy CJ. A visuospatial variant of mild cognitive impairment: getting lost between aging and AD. Neurology. 2003;60(5):802–8.

[155] Giannakopoulos P, Gold G, Duc M, Michel JP, Hof PR, Bouras C. Impaired processing of famous faces in Alzheimer's disease is related to neurofibrillary tangle densities in the prefrontal and anterior cingulate cortex. Dement Geriatr Cogn Disord. 2000;11(6): 336–41.

[156] Bokde AL, Lopez-Bayo P, Meindl T, Pechler S, Born C, Faltraco F, et al. Functional connectivity of the fusiform gyrus during a face-matching task in subjects with mild cognitive impairment. Brain. 2006;129(Pt 5):1113–24. DOI: 10.1093/brain/awl051.

[157] Takahashi S, Yonezawa H, Takahashi J, Kudo M, Inoue T, Tohgi H. Selective reduction of diffusion anisotropy in white matter of Alzheimer disease brains measured by 3.0 Tesla magnetic resonance imaging. Neurosci Lett. 2002;332(1):45–8.

[158] Silver MA, Kastner S. Topographic maps in human frontal and parietal cortex. Trends Cogn Sci. 2009;13(11):488–95. DOI: 10.1016/j.tics.2009.08.005.

[159] Swisher JD, Halko MA, Merabet LB, McMains SA, Somers DC. Visual topography of human intraparietal sulcus. J Neurosci. 2007;27(20):5326–37. DOI: 10.1523/JNEUROSCI.0991-07.2007.

[160] Sereno MI, Pitzalis S, Martinez A. Mapping of contralateral space in retinotopic coordinates by a parietal cortical area in humans. Science. 2001;294(5545):1350–4. DOI: 10.1126/science.1063695.

[161] Silver MA, Ress D, Heeger DJ. Topographic maps of visual spatial attention in human parietal cortex. J Neurophysiol. 2005;94(2):1358–71. DOI: 10.1152/jn.01316.2004.

[162] Ringman JM, Younkin SG, Pratico D, Seltzer W, Cole GM, Geschwind DH, et al. Biochemical markers in persons with preclinical familial Alzheimer disease. Neurology. 2008;71(2):85–92. DOI: 10.1212/01.wnl.0000303973.71803.81.

[163] Graham DP, Cully JA, Snow AL, Massman P, Doody R. The Alzheimer's Disease Assessment Scale-Cognitive subscale: normative data for older adult controls. Alzheimer Dis Assoc Disord. 2004;18(4):236–40.

[164] Tabert MH, Manly JJ, Liu X, Pelton GH, Rosenblum S, Jacobs M, et al. Neuropsychological prediction of conversion to Alzheimer disease in patients with mild cognitive impairment. Arch Gen Psychiatry. 2006;63(8):916–24. DOI: 10.1001/archpsyc.63.8.916.

[165] Saygin AP, Sereno MI. Retinotopy and attention in human occipital, temporal, parietal, and frontal cortex. Cereb Cortex. 2008;18(9):2158–68. DOI: 10.1093/cercor/bhm242.